eman ta zabal zazu

Universidad del País Vasco | Euskal Herriko Unibertsitatea

Shortcuts to adiabaticity and heat transport in trapped ions

Miguel Ángel Simón Martínez

Supervisors:

Prof. Juan Gonzalo Muga Francisco

Prof. Maria Luisa Pons Barba

Departamento de Química-Física

Facultad de Ciencia y Tecnología

Universidad del País Vasco/Euskal Herriko Unibertsitatea

(UPV/EHU)

Leioa, Febrero 2021

"Insert deep/meaningful/clever quote by someone who you admire or hate"

Someone who you admire or hate

Acknowledgements

Do not forget about the people that has been by your side and supported you.
Esta Tesis ha sido financiada a través de una beca predoctoral concedida por el Gobierno Vasco/Eusko Jaurlaritza

Contents

Acknowledgements **v**

List of Figures **ix**

List of publications **xiii**

Introduction **1**

1 Chapter Title **3**
- 1.1 Introduction . . . 4
- 1.2 Physical System . . . 6
- 1.3 Calculation of the stationary heat currents . . . 8
  - 1.3.1 Algebraic, small-oscillations approach to calculate the steady state . . . 10
- 1.4 Numerical Results . . . 12
  - 1.4.1 Evolution to steady state . . . 13
  - 1.4.2 Rectification in frequency graded chains . . . 14
  - 1.4.3 Same bath temperatures, different bath couplings . . . 15
  - 1.4.4 Dependence with ion number . . . 15
  - 1.4.5 Graded versus segmented . . . 16
- 1.5 Summary and discussion . . . 16

2 Rectification in a toy model **25**
- 2.1 Introduction . . . 26
- 2.2 Physical Model . . . 27
- 2.3 Covariance matrix in the steady state . . . 29
- 2.4 Solutions . . . 31
- 2.5 Relation of the Model to a trapped ion set-up . . . 33
  - 2.5.1 Collective trap . . . 33
  - 2.5.2 Individual on-site traps . . . 34
  - 2.5.3 Optical molasses and Langevin baths . . . 35
- 2.6 Looking for rectification . . . 36
  - 2.6.1 Parametric exploration . . . 38
  - 2.6.2 Spectral match/mismatch approach to rectification . . . 40
- 2.7 Conclusions . . . 43

2.8 acknowledgements 44
.1 Full set of steady-state equations for the components of $\mathbb{C}^{s.s}$ 45
.2 Complete expressions for the Spectral Density Matrix 45

Conclusions **47**

A Interaction versus asymmetry for adiabatic following **51**

Bibliography **53**

List of Figures

1.1 Schematic representation of the frequency-graded chain of trapped ions proposed as a thermal rectifier. The left and right ends of the chain are in contact with optical molasses at temperatures T_L and T_R (green and grey boxes respectively). Each ion is in an individual trap. The (angular) frequencies of the traps increase homogeneously from left to right, starting from ω_1 and ending at $\omega_1 + \Delta\omega$. The ions interact through the Coulomb force, which is long range, and therefore all the ions interact among them, even distant neighbors. By default we use 15 ions. 4

1.2 (a) Temperatures of the ions in the stationary state for a graded chain with the parameters described in section 1.4.1. The temperature profiles found with the algebraic method (Eq. (1.17)) are indistinguishable from the ones found solving the Langevin equation (Eq. (1.3)). Empty triangles (squares) correspond to $T_L = T_H$ ($T_L = T_C$) and $T_R = T_C$ ($T_R = T_H$). (b) Heat currents as a function of time for $T_L = T_H$ and $T_R = T_C$, see Eq. (1.9): $J_L(t)$ (solid green line) from the left reservoir into the chain; $J_R(t)$ (dotted grey line) from the right reservoir into the chain (negative except at very short times); $J_L(t) + J_R(t)$ (dotted-dashed black line), which must go to zero in the steady state. The three lines tend to stationary values marked by horizontal lines. Parameters: $\omega_1 = 2\pi \times 50$ kHz, $a = 50\,\mu$m, $\delta_H = -0.02\,\Gamma$, and $\delta_C = -0.1\,\Gamma$, which gives temperatures $T_H \approx 12$ mK and $T_C \approx 3$ mK. $\Delta\omega = 0.5\,\omega_1$. In all figures $\Gamma = 2\pi \times 41.3$ MHz. 18

1.3 Graded chain of $N = 15$ $^{24}Mg^+$ ions. (a) Stationary fluxes for different frequency increments: $J_\rightarrow$ (for $T_L = T_H$ and $T_R = T_C$, dashed line); $J_\leftarrow$ (for $T_L = T_C$ and $T_R = T_H$, solid line) (b) Rectification factor. Parameters: $\omega_1 = 2\pi \times 1$ MHz, $l = 5.25$ μm, $a = 4.76\,l$ (25 μm), $\delta_H = -0.02\,\Gamma$, and $\delta_C = -0.1\,\Gamma$. 19

1.4 Rectification factor in a graded chain of $N = 15$ $^{24}Mg^+$ ions for different trap distances and frequency increment. The dashed lines are for $R = 0$ and delimit the regions $J_\rightarrow > J_\leftarrow$ and $J_\rightarrow < J_\leftarrow$. The parameters are $\omega_1 = 2\pi \times 1$ MHz, $l = 5.25\,\mu$m, $\delta_H = -0.02\,\Gamma$, and $\delta_C = -0.1\,\Gamma$. 20

1.5 (a) Friction coefficient defined in Eq. (1.4). (b) Bath temperature defined in Eq. (1.5). (c) Rectification as a function of the temperature difference between the hot and cold baths $T_H - T_C$ for δ_H below (dashed black line) and above (solid blue line) the Doppler limit, and $\delta_C = \delta_D$ (Doppler limit). Parameters: $\omega_1 = 2\pi \times 1$ MHz, $\Delta\omega = 0.15\,\omega_1$, $l = 5.25\,\mu$m, $a = 4.76\,l$. 21
1.6 Rectification factor for different bath temperature differences ΔT as the number of ions is increased. The detuning of the cold bath laser is set to the Doppler limit $\delta_C = -\Gamma/2$. $\omega_1 = 2\pi \times 1$ MHz, $\Delta\omega = 0.15\,\omega_1$, $l = 5.25\,\mu$m, $a = 4.76\,l$. 22
1.7 Comparison of graded and segmented chains with $N = 15$ $^{24}Mg^+$ ions. (a) Maximum of $J_\rightarrow$ and $J_\leftarrow$ for the graded and segmented chain for different frequency increments. (b) Rectification factor: graded chain (dashed lines); segmented chain (solid lines). Parameters: $\omega_1 = 2\pi \times 1$ MHz, $l = 5.25\,\mu$m, $a = 4.76\,l$, $\delta_H = -0.02\,\Gamma$, and $\delta_C = -0.1\,\Gamma$. 23
1.8 Thermal conductivity through the chain for $T_L > T_R$ (empty squares), and $T_L < T_R$ (filled triangles). $\omega_1 = 2\pi \times 1$ MHz, $\Delta\omega = 0.15\,\omega_1$, $l = 5.25\,\mu$m, $a = 4.76\,l$, $\delta_H = -0.02\,\Gamma$ and $\delta_C = -0.1\,\Gamma$. 24

2.1 Diagram of the model described in Section 2.2. Two ions coupled to each other through a spring constant k. Each ion is harmonically trapped and connected to a bath characterized by its temperature T_i and its friction coefficient γ_i. 27
2.2 Rectification, R, in the $k_L k_R$ plane for $k = 1.17\times$ fN/m, $\gamma_L = 6.75 \times 10^{-22}$ kg/s, and $\gamma_R = 4.64\gamma_L$. 37
2.3 Rectification factor, R, given by Eq. (2.32). 40
2.4 Rectification for different values of $c = m_2/m_1 = \gamma_R/\gamma_L$ when the maximum condition in the $k_L k_R$ plane is satisfied (Eq. (2.31)). . . . 41
2.5 Spectral densities of the velocities of the ions (r_3 and r_4) corresponding to different values of c in Fig. 2.4: (a), (b) for $c = 1$ and (c), (d) for $c = 10$. Solid, black lines correspond to the left ion velocity spectral density $\mathbb{S}_{3,3}(\omega)$ and dashed, blue lines correspond to the right ion velocity spectral density $\mathbb{S}_{4,4}(\omega)$. (a) and (b) correspond to $R = 0$: the overlap between the phonon bands is the same in the forward and reversed configurations. (c) and (d) correspond to $R \approx 0.8$: in the forward configuration (c) the phonons match better than in the reversed configuration (d). 42

dedicatory here

List of publications

I) **The results of this Thesis are based on the following articles**

Published Articles

1. E. Torrontegui, S. Martínez-Garaot, A. Ruschhaupt, and J. G. Muga
   Shortcuts to adiabaticity: Fast-forward approach
   Phys. Rev. A **86**, 013601 (2012).

II) **Other articles produced during the Thesis period**

Published Articles not included in this Thesis

2. S. Ibáñez, S. Martínez-Garaot, X. Chen, E. Torrontegui, and J. G. Muga
   Shortcuts to adiabaticity for non-Hermitian systems
   Phys. Rev. A **84**, 023415 (2011).

Introduction

Todo fuego que se precie empieza con una pequeña chispa.

Reid

Chapter 1

Chapter Title

We numerically demonstrate heat rectification for linear chains of ions in trap lattices with graded trapping frequencies, in contact with thermal baths implemented by optical molasses. To calculate the local temperatures and heat currents we find the stationary state by solving a system of algebraic equations. This approach is much faster than the usual method that integrates the dynamical equations of the system and averages over noise realizations.

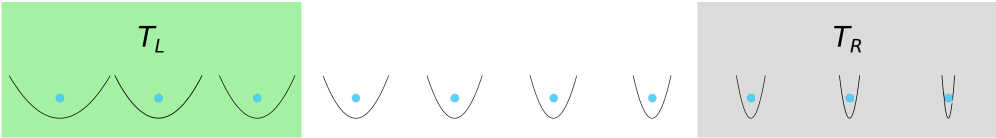

FIGURE 1.1: Schematic representation of the frequency-graded chain of trapped ions proposed as a thermal rectifier. The left and right ends of the chain are in contact with optical molasses at temperatures T_L and T_R (green and grey boxes respectively). Each ion is in an individual trap. The (angular) frequencies of the traps increase homogeneously from left to right, starting from ω_1 and ending at $\omega_1 + \Delta\omega$. The ions interact through the Coulomb force, which is long range, and therefore all the ions interact among them, even distant neighbors. By default we use 15 ions.

1.1 Introduction

The ideal thermal rectifier, also "thermal diode", is a device that allows heat to propagate in one direction, from a hot to a cold bath, but not in the opposite one when the temperature bias of the baths is reversed. The name is set by analogy to the half-wave rectifiers or diodes for electric current. More generally thermal rectification simply denotes asymmetric heat flows (not necessarily all or nothing) when the bath temperatures are reversed. Thermal rectification was discovered by C. Starr in 1936 in a junction between copper and cuprous oxide [1]. Many years later, a work of Terraneo *et al.* demonstrated thermal rectification in a model consisting on a segmented chain of coupled nonlinear oscillators in contact with two thermal baths at temperatures T_H and T_C, with $T_H > T_C$ [2]. This paper sparked a substantial body of research that spans to this day [3] (see Fig. 1 in [4]).

Research on thermal rectification has gained a lot of attention in recent years as a key ingredient to build prospective devices to control heat flows similarly to electrical currents [4, 5]. There are proposals to engineer thermal logic circuits [6] in which information, stored in thermal memories [7], would be processed in thermal gates [8]. Such thermal gates, as their electronic counterparts, will require thermal diodes and thermal transistors to operate [9, 10]. Heat rectifying devices would also be quite useful in nano electronic circuits, letting delicate components dissipate heat while being protected from external heat sources [4].

Most work on thermal diodes has been theoretical with only a few experiments [11–14]. A relevant attempt to build a thermal rectifier was based on a graded structure made of carbon and boron nitride nanotubes that transports heat between a pair of heating/sensing circuits [11]. One of the ends of the nanotube is loaded with a deposition of another material, which makes the heat flow better from the loaded end to the unloaded end. However, rectifications were small, with rectification factors (relative heat-flow differentials) around 7%.

Much effort has been aimed at improving the rectification factors and the features of the rectifiers. Some works relied, as in [2], on a chain segmented into two or more regions with different properties, but using other lattice models such as the Frenkel-Kontorova (FK) model [15, 16]. The fundamental ingredient for having rectification was attributed to nonlinear forces in the chain [5, 15–19], which lead to a temperature dependence of the phonon bands or power spectral densities. The bands may match or mismatch at the interfaces depending on the sign of the temperature bias of the baths, allowing or obstructing heat flow [2, 20]. Later, alternative mechanisms have been proposed which do not necessarily rely on anharmonic potentials [21, 22]. Also, Peyrard provided a simple model to explain and build rectifiers based on assuming the Fourier law for heat conduction locally combined with a temperature and position-dependent conductivity [23].

It was soon realized that the performance of segmented rectifiers was very sensitive to the size of the device, i.e., rectification decreases with increasing the length of the rectifier [16]. To overcome this limitation two ideas were proposed. The first one consists in using graded rather than segmented chains, i.e., chains where some physical property varies continuously along the site position such as the mass of particles in the lattice [24–32]. The second one uses particles with long-range interactions (LRI), such that all the particles in the lattice interact with each other [25, 33, 34]. The rationale behind was that in a graded system new asymmetric, rectifying channels are created, while the long-range interactions create also new transport channels, avoiding the usual decay of heat flow with size [25]. Besides a stronger rectification power, LRI graded chains are expected to have better heat conductivity than segmented ones. This is an important point for technological applications, because devices with high rectification factors are not useful if the currents that flow through them are very small.

In this article we propose to bridge the gap between mathematical models and actual systems exploring the implementation of a heat rectifier in a realistic, graded system with long-range interactions: a chain of ultracold ions in a segmented Paul trap with graded microtraps for each ion. Long-range interactions are due to the

Coulomb forces, and the baths at the ends of the chain may be implemented with optical molasses, see Fig. 1.1. The trapping frequencies of the microtraps are controlled individually in order to create a graded and asymmetric trap-frequency profile along the chain. This asymmetry will lead to a heat flow that depends on the sign of the temperature difference of the baths. Heat transport in trapped ion chains has been studied in several works [35–39] and interesting phenomena like phase transitions have been investigated [35–38]. The idea of using locally-controlled traps is already mentioned in [35] to implement disorder and study its effects. The device we present here may be challenging to implement, but at reach with the current technology, in particular that of microfabricated traps [40–42]. Thus the setting is thought for a small, realistic number of controllable ions.

The rest of the article is organized as follows. In Section 1.2 we describe the physical system of trapped ions with graded trap frequencies. We also set the stochastic dynamics due to the action of lasers at the chain edges. In Section 1.3 we implement an efficient method to find the steady state using Novikov's theorem and solving an algebraic system of equations. In Section 1.4 we present simulations of this system exhibiting thermal rectification and discuss the dependence with ion number, different options for the ion-laser coupling, and the advantages/disadvantages of using a graded frequency profile instead of a segmented one. Finally, in Section 1.5 we summarize our conclusions, and discuss connections with other works.

1.2 Physical System

Consider a linear lattice of N individual harmonic traps of (angular) trapping frequencies ω_n evenly distributed along the x axis at a distance a from each other. Each trap contains a single ion that interacts with the rest via Coulomb potentials. All the ions are of the same species, with mass m and charge q. The Hamiltonian that describes the dynamics of the system is (we consider only linear, one dimensional motion along the chain axis)

$$H(\boldsymbol{x},\boldsymbol{p}) = \sum_{n=1}^{N}\left[\frac{p_n^2}{2m} + \frac{m\omega_n^2}{2}(x_n - x_n^{(0)})^2\right] + V_{int}(\boldsymbol{x}), \tag{1.1}$$

where $\{x_n, p_n\}$, position and momentum of each ion, are the components of the vectors $\boldsymbol{x}, \boldsymbol{p}$, $x_n^{(0)} = na$ are the centers of the harmonic traps, and V_{int} is the sum of the Coulomb interaction potential between all pairs of ions,

$$V_{int}(\boldsymbol{x}) = \frac{1}{2}\sum_{n}\sum_{l\neq n} V_C(|x_n - x_l|), \tag{1.2}$$

with $V_C(|x_n - x_l|) = \frac{q^2}{4\pi\varepsilon_0}\frac{1}{|x_n-x_l|}$. The ends of the chain are in contact with two thermal reservoirs at temperatures T_L for the left bath and T_R for the right bath respectively. The action of the resevoirs on the dynamics of the chain is modeled via Langevin baths at temperatures T_L and T_R [43, 44]. The equations of motion of the chain, taking into account the baths and the Hamiltonian, are

$$\begin{aligned}\dot{x}_n &= \frac{1}{m}p_n,\\ \dot{p}_n &= -m\omega_n^2(x_n - x_n^{(0)}) - \frac{\partial V_{int}}{\partial x_n} - \frac{\gamma_n}{m}p_n + \xi_n(t),\end{aligned} \tag{1.3}$$

where γ_n and $\xi_n(t)$ are only non-zero for the ions in the end regions, in contact with the left and right baths in the sets $\mathcal{L} = \{1, 2, ..., N_L\}$ and $\mathcal{R} = \{N - (N_R - 1), ..., N - 1, N\}$, see Fig. 1.1. The γ_n are friction coefficients and $\xi_n(t)$ are uncorrelated Gaussian noise forces satisfying $\langle\xi_n(t)\rangle = 0$ and $\langle\xi_n(t)\xi_m(t')\rangle = 2D_n\delta_{nm}\delta(t - t')$, D_n being the diffusion coefficients. These Gaussian forces are formally the time derivatives of independent Wiener processes (Brownian motions) $\xi_n(t) = \sqrt{2D_n}\frac{dW_n}{dt}$ [36, 45] and Eq. (1.3) is a stochastic differential equation (SDE) in the Stratonovich sense [45].

The baths are physically implemented by optical molasses consisting of a pair of counterpropagating Doppler-cooling lasers [36]. The friction and diffusion coefficients for the ions in contact with the baths are given by [36, 46, 47]

$$\begin{aligned}\gamma_n &= -4\hbar k_{L,R}^2\left(\frac{I_{L,R}}{I_0}\right)\frac{2\delta_{L,R}/\Gamma}{[1 + (2\delta_{L,R}/\Gamma)^2]^2},\\ D_n &= \hbar^2 k_{L,R}^2\left(\frac{I_{L,R}}{I_0}\right)\frac{\Gamma}{1 + (2\delta_{L,R}/\Gamma)^2},\\ & n \in \mathcal{L}, \mathcal{R},\end{aligned} \tag{1.4}$$

where k_L (k_R) and I_L (I_R) are the wave vector and intensity of the left (right) laser. δ_L (δ_R) is the detuning of the left (right) laser with respect to the angular frequency ω_0 of the atomic transition the laser is exciting, and Γ is the corresponding natural line width of the excited state. The expressions in Eq. (1.4) are valid only if the intensities of the lasers are small compared to the saturation intensity I_0, $I_{L,R}/I_0 \ll 1$. In this bath model, the friction term in Eq. (1.3) comes from the cooling action of the laser and the white noise force $\xi_n(t)$ corresponds to the random recoil of the ions due to spontaneous emission of photons [46, 47]. Using the diffusion-dissipation relation $D = \gamma k_B T$ [48], the temperatures of the optical molasses baths are given by

$$T_{L,R} = -\frac{\hbar\Gamma}{4k_B}\frac{1 + (2\delta_{L,R}/\Gamma)^2}{(2\delta_{L,R}/\Gamma)}, \tag{1.5}$$

with k_B being the Boltzmann constant. If the laser intensities are low enough, the temperatures of the baths are controlled by modifying the detunings. When $\delta = \delta_D = -\Gamma/2$ the optical molasses reach their minimum temperature possible, the Doppler limit $T_D = \hbar\Gamma/(2k_B)$. Note that away from the Doppler limit the same temperature may be achieved for two different values of detuning. These two possibilities imply different couplings (two different pairs of γ and D values) and thus different physical effects that will be studied in Sec. 1.4.3.

1.3 Calculation of the stationary heat currents

The local energy of each site is defined by

$$H_n = \frac{1}{2m}p_n^2 + \frac{1}{2}m\omega_n^2\left(x_n - x_n^{(0)}\right)^2 + \frac{1}{2}\sum_{l\neq n} V_C(|x_n - x_l|). \tag{1.6}$$

Differentiating H_n with respect to time we find the continuity equation

$$\dot{H}_n = \frac{p_n}{m}\left[\xi_n(t) - \gamma_n\frac{p_n}{m}\right] - \frac{1}{2m}\sum_{l\neq n}\frac{\partial V_C(|x_n - x_l|)}{\partial x_n}(p_n + p_l). \tag{1.7}$$

Two different contributions can be distinguished: $j_n^B \equiv \frac{p_n}{m}\left[\xi_n(t) - \gamma_n\frac{p_n}{m}\right]$, which is the energy flow from the laser reservoir to the ions at the edges of the chain (only for $n \in \mathcal{L}, \mathcal{R}$), and $\dot{H}_n^{int} \equiv -\frac{1}{2m}\sum_{l\neq n}\frac{\partial V_C(|x_n - x_l|)}{\partial x_n}(p_n + p_l)$, which gives the "internal" energy flow due to the interactions with the rest of the ions. In the steady state $\left\langle \dot{H}_n \right\rangle = 0$, and therefore

$$\left\langle j_n^B \right\rangle + \left\langle \dot{H}_n^{int} \right\rangle = 0, \tag{1.8}$$

where $\langle\cdots\rangle$ stands for the expectation value with respect to the ensemble of noise processes $\boldsymbol{\xi}(t)$ ($\boldsymbol{\xi}$ represents a vector with components ξ_n). Equation (1.8) implies that, in the steady state, the internal rates $\dot{H}_n^{int}$ vanish for the inner ions of the chain because $j_n^B = 0$ for $n \notin \mathcal{L}, \mathcal{R}$. In chains with nearest-neighbor (NN) interactions, $\langle \dot{H}_n^{int} \rangle$ simplifies to two compensating and equal-in-magnitude contributions that define the homogeneous heat flux across the chain. For long-range interactions this is not so and defining the flux is not so straightforward. A formal possibility is to impose nearest-neighbor interatomic interactions for some atoms in the chain [25], but this approach is not realistic in the current system so we define instead the heat currents for the left and right baths as

$$
\begin{aligned}
J_L(t) &= \sum_{n\in\mathcal{L}} \left\langle j_n^B \right\rangle, \\
J_R(t) &= \sum_{n\in\mathcal{R}} \left\langle j_n^B \right\rangle,
\end{aligned}
\tag{1.9}
$$

respectively. These expressions are in general time-dependent. In the steady state we must have $J_{L,\text{steady}} + J_{R,\text{steady}} = 0$, since the local energies stabilize and internal energy flows cancel. We use either $J_{L,\text{steady}}$ or $J_{R,\text{steady}}$ to calculate the total energy flow in the chain, always taking the absolute value, i.e., $J \equiv |J_{L,\text{steady}}| = |J_{R,\text{steady}}|$. J is defined as $J_{\rightarrow}$ when the hot bath is on the left and $J_{\leftarrow}$ when it is on the right.

To compute the average heat fluxes of the baths $\left\langle j_n^B \right\rangle$ in Eq. (1.9) we need the averages $\langle p_n(t)\xi_n(t)\rangle$. Instead of explicitly averaging $p_n(t)\xi_n(t)$ over different realizations of the white noise we use Novikov's theorem [45, 49, 50]. Novikov's theorem states that the ensemble average (over the realizations of the noise) of the product of some functional $\phi(t)$, which depends on a Gaussian noise $\xi(t)$ with zero mean value, $\langle\xi(t)\rangle = 0$, and the noise itself, is given by

$$
\langle \xi(t)\phi(t)\rangle = \int_0^t dt' \,\langle \xi(t)\xi(t')\rangle \left\langle \frac{\delta\phi(t)}{\delta\xi(t')} \right\rangle, \tag{1.10}
$$

where $\delta\phi(t)/\delta\xi(t')$ is the functional derivative of $\phi(t)$ with respect to the noise, with $t' < t$. When the noise is $\delta-$correlated, $\langle\xi(t)\xi(t')\rangle = 2D\delta(t-t')$, and Eq. (1.10) reads $\langle\xi(t)\phi(t)\rangle = D\,\langle\delta\phi(t)/\delta\xi(t')\rangle\,|_{t'\to t^-}$. To apply Novikov's theorem to our model we need the functional derivatives of the position $x_n(t)$ and momentum $p_n(t)$ coordinates with respect to the white noises. We integrate Eq. (1.3) to have its formal solution as a functional depending on the white Gaussian noises $\xi_n(t)$,

$$\begin{aligned} x_n(t) &= x_n(0) + \frac{1}{m}\int_0^t ds\; p_n(s), \\ p_n(t) &= p_n(0) + \int_0^t ds\; \left[-\frac{\partial H}{\partial x_n}(s) - \frac{\gamma_n}{m} p_n(s) + \xi_n(s) \right]. \end{aligned} \tag{1.11}$$

Equation (1.11) implies that the functional derivatives are $\delta x_n(t)/\delta\xi_m(t')|_{t'\to t^-} = 0$ and $\delta p_n(t)/\delta\xi_m(t')|_{t'\to t^-} = \delta_{nm}$ (δ_{nm} is the usual Kronecker delta symbol). Thus we have $\langle x_n(t)\xi_m(t)\rangle = 0$ and $\langle p_n(t)\xi_m(t)\rangle = \delta_{nm} D_m$, which gives for the heat flow from the baths

$$\langle j_n^B \rangle = \frac{1}{m}\left[D_n - \gamma_n \frac{\langle p_n^2 \rangle}{m} \right]. \tag{1.12}$$

In all simulations we check that $|J_{L,\text{steady}}| = |J_{R,\text{steady}}|$ within the numerical tolerance of the computer. To measure the asymmetry of the heat currents we use the rectification factor R defined as

$$R = \frac{J_{\rightarrow} - J_{\leftarrow}}{max(J_{\rightarrow}, J_{\leftarrow})}. \tag{1.13}$$

R values may go from -1 to 1 (In the figures we depict it in % between -100% and 100%). If there is no rectification $J_{\rightarrow} = J_{\leftarrow}$ and $R = 0$. For perfect rectification in the right (left) direction, $J_{\rightarrow} \gg J_{\leftarrow}$ ($J_{\rightarrow} \ll J_{\leftarrow}$), and $R = 1$ ($R = -1$). Take note that other definitions of rectification factors exist in many works on asymmetric heat transfer so comparisons should be done with care.

This model does not show the antithermodynamical behavior observed in other models [51, 52], and heat is found to flow in all cases from the hot to the cold bath.

1.3.1 Algebraic, small-oscillations approach to calculate the steady state

To find the temperature profiles and heat currents in the steady state the usual approach is to solve the SDE system in Eq. (1.3) up to long times and for many realizations of the white noises $\boldsymbol{\xi}(t)$. In that way the ensemble averages $\langle p_n(t\to\infty)^2\rangle$, necessary for both the temperature profiles and heat currents, are computed. This standard route implies a heavy computational effort, in particular when we want to study the heat transport for several bath configurations, frequency increments and chain parameters. It is possible to circumvent this difficulty and find ensemble averages like $\langle x_n x_m \rangle$, $\langle x_n p_m \rangle$, $\langle p_n p_m \rangle$ (second order moments) without integrating any SDE [53]. The idea is to impose the condition $d\langle \cdots \rangle/dt = 0$ for all the second order moments and linearize the dynamical equations of the system around equilibrium. A system of linear algebraic equations for the moments results, that can be easily solved without solving the SDE many times.

To linearize the SDE in Eq. (1.3) we approximate the potential energy of the Hamiltonian in Eq. (1.1), $V(\boldsymbol{x}) = V_{int}(\boldsymbol{x}) + m \sum_n \omega_n^2 (x_n - x_n^{(0)})^2/2$, by its harmonic approximation around the equilibrium positions $\boldsymbol{x}^{eq}$, defined by $\left.\frac{\partial V(\boldsymbol{x})}{\partial \boldsymbol{x}}\right|_{\boldsymbol{x}=\boldsymbol{x}^{eq}} = 0$. The approximate potential (ignoring the zero-point energy) is

$$V(\boldsymbol{x}) \approx \frac{1}{2} \sum_{n,m} K_{nm} (x_n - x_n^{eq})(x_m - x_m^{eq}), \tag{1.14}$$

with $K_{nm} = \left.\frac{\partial^2 V(\boldsymbol{x})}{\partial x_n \partial x_m}\right|_{\boldsymbol{x}=\boldsymbol{x}^{eq}}$ being the Hessian matrix entries of $V(\boldsymbol{x})$ around the equilibrium configuration [54]

$$K_{nm} = \begin{cases} m\omega_n^2 + 2\left(\frac{q^2}{4\pi\varepsilon_0}\right) \sum_{l \neq n} \frac{1}{\left|x_n^{eq} - x_l^{eq}\right|^3} & \text{if } n = m \\ -2\left(\frac{q^2}{4\pi\varepsilon_0}\right) \frac{1}{\left|x_n^{eq} - x_m^{eq}\right|^3} & \text{if } n \neq m \end{cases}. \tag{1.15}$$

Note that this approximation does not modify the two main features of the system, namely asymmetry and long-range interactions, which are manifest in the asymmetric distribution of ω_n and the non-zero off-diagonal elements of the K matrix, respectively. In the following we will use $y_n = x_n - x_n^{eq}$ to simplify the notation. The linearized dynamics around the equilibrium positions are given by

$$\begin{aligned} \dot{y}_n &= \frac{1}{m} p_n, \\ \dot{p}_n &= -\sum_l K_{nl} y_l - \frac{\gamma_n}{m} p_n + \xi_n(t). \end{aligned} \tag{1.16}$$

Now, we set $d\langle \cdots \rangle/dt = 0$ for all the moments. Using Eq. (1.16) and applying Novikov's theorem we find

$$\begin{gathered} \langle p_n p_l \rangle - \gamma_l \langle y_n p_l \rangle - \sum_m K_{lm} \langle y_n y_m \rangle = 0, \\ \sum_m \left[K_{nm} \langle y_m p_l \rangle + K_{lm} \langle y_m p_n \rangle \right] + \frac{1}{m} (\gamma_l + \gamma_n) \langle p_n p_l \rangle = 2\delta_{nl} D_n. \end{gathered} \tag{1.17}$$

The system (1.17) is linear in the second order moments so it can be solved numerically to find the steady-state values of the moments. Besides Eq. (1.17) we have that $\langle y_n p_l \rangle = -\langle y_l p_n \rangle$, which follows from Eq. (1.16) and $d\langle y_n y_m \rangle/dt = 0$. Since there are $\frac{1}{2}N(N-1)$ independent $\langle y_n p_l \rangle$ moments, we choose the ones with $n < l$. Similarly, the moments $\langle y_n y_l \rangle$ and $\langle p_n p_l \rangle$ contribute with $\frac{1}{2}N(N+1)$ independent variables each and we choose the ones with $n \leq m$. Thus there are in total $\frac{1}{2}N(3N+1)$ independent moments that we arrange in the vector

$$\begin{aligned} \boldsymbol{\eta} = \Big[& \langle y_1 y_1 \rangle, \langle y_1 y_2 \rangle, ..., \langle y_N y_N \rangle, \\ & \langle p_1 p_1 \rangle, \langle p_1 p_2 \rangle, ..., \langle p_N p_N \rangle, \\ & \langle y_1 p_2 \rangle, \langle y_1 p_3 \rangle, ..., \langle y_{N-1} p_N \rangle \Big]^T. \end{aligned} \tag{1.18}$$

There are the same number of independent equations as independent moments: N^2 equations correspond to the first line in Eq. (1.17), and $\frac{1}{2}N(N+1)$ equations to the second line because of the symmetry with respect to n, l. The system of equations (1.17) may be compactly written as $\mathbf{A}\boldsymbol{\eta} = \mathbf{B}$, where $\mathbf{A}$ and $\mathbf{B}$ are a $\frac{1}{2}N(3N+1)$ square matrix and vector.

1.4 Numerical Results

We now display the results of our simulations. To find the temperature profiles and the currents in the steady state we use the algebraic method described in section 1.3.1. We also check that the results coincide with those by solving Eq. (1.3) for many different realizations of the noisy forces $\boldsymbol{\xi}(t)$ and averaging. The code for all the numerical simulations has been written in the language *Julia* [55, 56]. In particular, to solve the Langevin equation, we used *Julia*'s package *DifferentialEquations.jl* [57].

To model the baths and the chain we use atomic data taken from ion trap experiments [58, 59]. We consider 15 $^{24}\mathrm{Mg}^{+}$ ions in all figures except in Fig. 1.6. The three leftmost and three rightmost ions are illuminated by Doppler cooling lasers. The Doppler cooling lasers excite the transition $3s^2S_{1/2} \rightarrow 3p^2P_{1/2}$, with angular frequency $\omega_0 = 2\pi \times 1069$ THz and excited state line width $\Gamma = 2\pi \times 41.3$ MHz [36]. For this ionic species and atomic transition the Doppler limit is $T_D =$ 1 mK. The intensities of the laser beams are small compared to the saturation intensity I_0 so that Eq. (1.4) holds. We take $I_n/I_0 = 0.08$ for the ions in the laser beams, whereas $I_n = 0$ for the rest.

The temperatures T_L, T_R of the left and right laser baths are controlled with their detunings δ_L, δ_R with respect to the atomic transition. We fix two values for the detunings, δ_H and δ_C, such that $T_H > T_C$ (hot and cold baths, also source and drain) and we define $J_{\rightarrow}$ ($J_{\leftarrow}$) as the stationary heat current in the chain when $T_L = T_H$ and $T_R = T_C$ ($T_L = T_C$ and $T_R = T_H$).

Except in Sec. 1.4.5 we consider a graded frequency profile. If the frequency of the leftmost trap is ω_1, the frequency of the nth trap will be $\omega_n = \omega_1 + \Delta\omega\frac{n-1}{N-1}$ up to $\omega_1 + \Delta\omega$ for the rightmost trap. In Sec. 1.4.5 we compare the graded chain to a segmented chain, where the left half of the chain has trapping frequencies ω_1 while the other half has $\omega_1 + \Delta\omega$.

1.4.1 Evolution to steady state

To compare the results by solving Eq. (1.3) and averaging and those from the algebraic method we simulated a frequency graded chain with a trapping frequency $\omega_1 = 2\pi \times 50$ kHz for the leftmost ion, see Fig. 1.2. The number of ions interacting with the laser beams (three on each bath) is consistent with the lattice constant and typical waists of Gaussian laser beams [58, 59]. To set the trap distance we fix first the characteristic length $l = \left(\frac{q^2}{4\pi\varepsilon_0}\frac{1}{m\omega_1^2}\right)^{1/3}$ as the distance for which the Coulomb repulsion of two ions equals the trap potential energy for an ion at a distance l away from the center of its trap. If $a < l$, the Coulomb repulsion of the ions is stronger than the trap confinement which makes the ions jump from their traps. With the parameters used in this section we have $l = 38.7\,\mu$m and set $a = 1.29\,l = 50\,\mu$m. The detunings of the *hot* and *cold* lasers are $\delta_H = -0.02\,\Gamma$, and $\delta_C = -0.1\,\Gamma$ which gives temperatures $T_H \approx 12$ mK and $T_C \approx 3$ mK. We fix the value $\Delta\omega = 0.5\,\omega_1$ for the frequency increment.

The results of the two methods are in very good agreement. In the scale of Fig. 1.2 (a) the calculated local temperatures are undistinguishable. In the calculation based on solving the dynamics we had to integrate Eq. (1.3) for $N_{trials} = 1000$ realizations of white noise $\boldsymbol{\xi}(t)$. The method based on the system of moments shortened the calculation time with respect to the dynamical trajectories by a factor of 1/700. In fact, the time gain is even more important because the dynamical method requires further processing, performing a time averaging to compute the stationary flux in addition to noise averaging, see Fig. 1.2 (b).

Additionally, the relaxation to the steady state slows down when the frequencies of the traps increase since the deterministic part of the Langevin equation dominates the dynamics over the stochastic part, entering an under-damped regime. In contrast, this increase does not affect the algebraic method.

1.4.2 Rectification in frequency graded chains

In this subsection we demonstrate rectification for the frequency graded chain. We used the method described in section 1.3.1 for $^{24}Mg^+$ ions with the same parameters for the baths used before. We fix the trapping frequency of the leftmost trap to $\omega_1 = 2\pi \times 1$ MHz, and a trap spacing $a = 4.76\, l$ ($25\,\mu$m) (the characteristic length is $l = 5.25\,\mu$m). Figure 1.3 depicts the results with these parameters in a graded chain. Figure 1.3 (a) shows that both $J_\rightarrow$ and $J_\leftarrow$ decrease rapidly as the frequency increment is increased. The rectification reaches its maximum value for a frequency difference of $\Delta\omega \approx 0.1\omega_1$. The fluxes cross so there are some points where the rectification is exactly zero, besides the trivial one at $\Delta\omega = 0$, at $\Delta\omega = 0.05\,\omega_1,\ 0.3\,\omega_1,\ 1.3\,\omega_1$. At these points the direction of rectification reverses, presumably as a consequence of the changes in the match/mismatch of the temperature dependent local power spectra. The change of rectification direction occurs for all the choices of parameters, as displayed in Fig. 1.4. Figure 1.4 gives the rectification factor for different trap distances and frequency increments. 0-rectification curves separate regions with different rectification direction. The second region in Fig. 1.4 (starting from the left) would be the most interesting one to build a thermal diode, since rectification reaches its largest values there.

For small values of $\Delta\omega$ there is little asymmetry in the chain and therefore modest rectification is expected whereas a very large $\Delta\omega$ implies very high trapping frequencies on the right implying too strong a confinement and vanishing interactions. This bottleneck decreases the fluxes in both directions and the rectification. However, since $\Delta\omega$ is controllable, and the range of values of $\Delta\omega$ for which rectification is larger can be also controlled with the intertrap distance a, see Fig. 1.4, the existence of a rectification window does not imply a major limitation.

1.4.3 Same bath temperatures, different bath couplings

As already mentioned below Eq. (1.5), above and below the detuning $\delta_D = -\Gamma/2$ corresponding to the Doppler limit temperature, the optical molasses allow for two different couplings (two pairs of friction and diffusion coefficients in Eq. (1.4)) between the ions and the laser corresponding to the same bath temperature. This duality may be seen explicitly in Fig. 1.5. Specifically Fig. 1.5 (a) depicts the variation of the friction coefficient for values of δ around δ_R, and Fig. 1.5 (b) the corresponding temperatures. Interestingly, the different couplings imply different rectification factors. If we set $\delta_C = \delta_D = -\Gamma/2$, i.e., the cold bath is cooled to the Doppler limit, δ_H can be chosen to be below or above δ_D for the same temperature T_H. The corresponding rectification factors for the two choices are shown in Fig. 1.5 (c), which demonstrates that significant rectification can be achieved by choosing $\delta_H < \delta_D$ for temperature increments that are smaller than or of the order of $T_C = T_D$, for example $R \approx 20\%$ for $\Delta T = 0.1T_C$, or $R \approx 60\%$ for $\Delta T = T_C$. Finding good rectification at low (relative) temperature differences is considered to be one on the challenges in asymmetric heat transport research [60].

1.4.4 Dependence with ion number

Keeping in mind that scaling the frequency-graded ion chain to a large numbers of ions is not a realistic option in this setting, it is nevertheless important to study the dependence with ion number from small to moderate numbers. In Fig. 1.6 we observe an overall trend in which the rectification decreases with the number of ions in the chain (while it increases with temperature bias ΔT in the studied range). This effect is easy to understand, as increasing N while keeping the total variation of the trapping frequency $\Delta\omega$ constant, the frequency gradient decreases. This lowers the asymmetry in the chain and the rectification factor. Oscillations with N superimposed to the global trend are more visible at the smaller N values giving an optimal N value at $N = 19$.

1.4.5 Graded versus segmented

We have also compared the performance of the graded thermal diode and a segmented version in which the left half of the chain is trapped with frequency ω_1 and the right half (including the middle ion) with $\omega_1 + \Delta\omega$. Even though the optimal rectification in Fig. 1.7 (a) for the segmented chain is larger than for the graded chain, the fact that the fluxes are generally much larger for the graded chain, see Fig. 1.7 (b), makes the graded chain more interesting for applications.

1.5 Summary and discussion

In this article we have numerically demonstrated heat rectification in a chain of ions trapped in individual microtraps with graded frequencies, connected at both ends to thermal baths created by optical molasses. An alternative to implement a graded frequency profile in the lab could be combining a collective Paul trap for all the ions with on-site dipolar laser forces [35, 61–63].

A goal of this article is to connect two communities, ion trappers and researchers on heat-rectification models. The results found are encouraging and demonstrate the potential of a trapped-ion platform to experimentally investigate heat rectification schemes. Trapped ions are quite interesting to this end because they are highly controllable, and may easily adopt several features to enhance rectification, such as the ones explored here (long-range interactions and an asymmetrical gradation), or others such as time dependent forces [5, 64], or different nonlinearities in onsite forces. The limitations and application domain should also be clear, the proposed platform is circumscribed to cold temperatures of the order of hundreds of μK to mK achieved by Doppler cooling. In this sense it is not aimed at competing with (it is rather complementary to) proposals for which experiments [11–14] or simulations [60, 65, 66] demonstrate thermal rectification at room temperature or for hundreds of K. Also, the number of ions should realistically be kept small so the proposed ion chain is not aimed at achieving a macroscopic diode length, but at playing a role in thermal diode research and in the context of ion-trapped based quantum technologies.

Methodologically, the calculation of the steady state has been performed with an algebraic approach much faster than the time-consuming integration and averaging over noise and time of the dynamical equations. The algebraic approach linearizes the forces around equilibrium positions which, in this system and for the realistic parameters considered is well justified and tested numerically. The results found provide additional evidence that simple linear models may rectify heat flow [21]. We underline that our linear model is, arguably, even simpler than some linear "minimalist, toy models" in [21] that showed rectification (our on-site forces are already linear from the start and the temperature dependence of explicit model parameters is only in the coefficients of the Langevin baths), with the important bonus of being also realistic.

To shed some more light on the mechanism behind the observed rectification we may analyze the local thermal conductivities $\lambda[x, T(x)]$ defined in a continuous model by [23]

$$J = \lambda[x, T(x)] \left| \frac{dT(x)}{dx} \right|, \tag{1.19}$$

where J is the stationary heat current and $T(x)$ the local temperature. (We use the modulus of the temperature derivative for consistency with our (positive) definition of J.) In our model we discretize the coordinate with the ion index and the temperature derivative is discretized as

$$\frac{dT_n}{dx} = \frac{T_{n+1} - T_{n-1}}{x^{eq}_{n+1} - x^{eq}_{n-1}}. \tag{1.20}$$

Through integration, it is clear that when λ depends on both temperature and position rectification is possible. In the continuous model the temperature increment between the baths is

$$|T_L - T_R| = \int_0^L \frac{J}{\lambda[x, T(x)]} dx \tag{1.21}$$

so that the key for rectification is a different integral of the inverse of the conductivities in the two scenarios ($T_L = T_H, T_R = T_C$ with conductivity $\lambda_{\rightarrow}[x, T_{\rightarrow}(x)]$ along a local temperature decreasing from the left or the reversed one, $T_R = T_H, T_L = T_C$ with conductivity $\lambda_{\leftarrow}[x, T_{\leftarrow}(x)]$ along an increasing local temperature. Particularly favorable for rectification is the scenario where one of the lambdas is above the other one for all x. Figure 1.8 shows that this is essentially the case in our model, at least along the most relevant part of the integral.

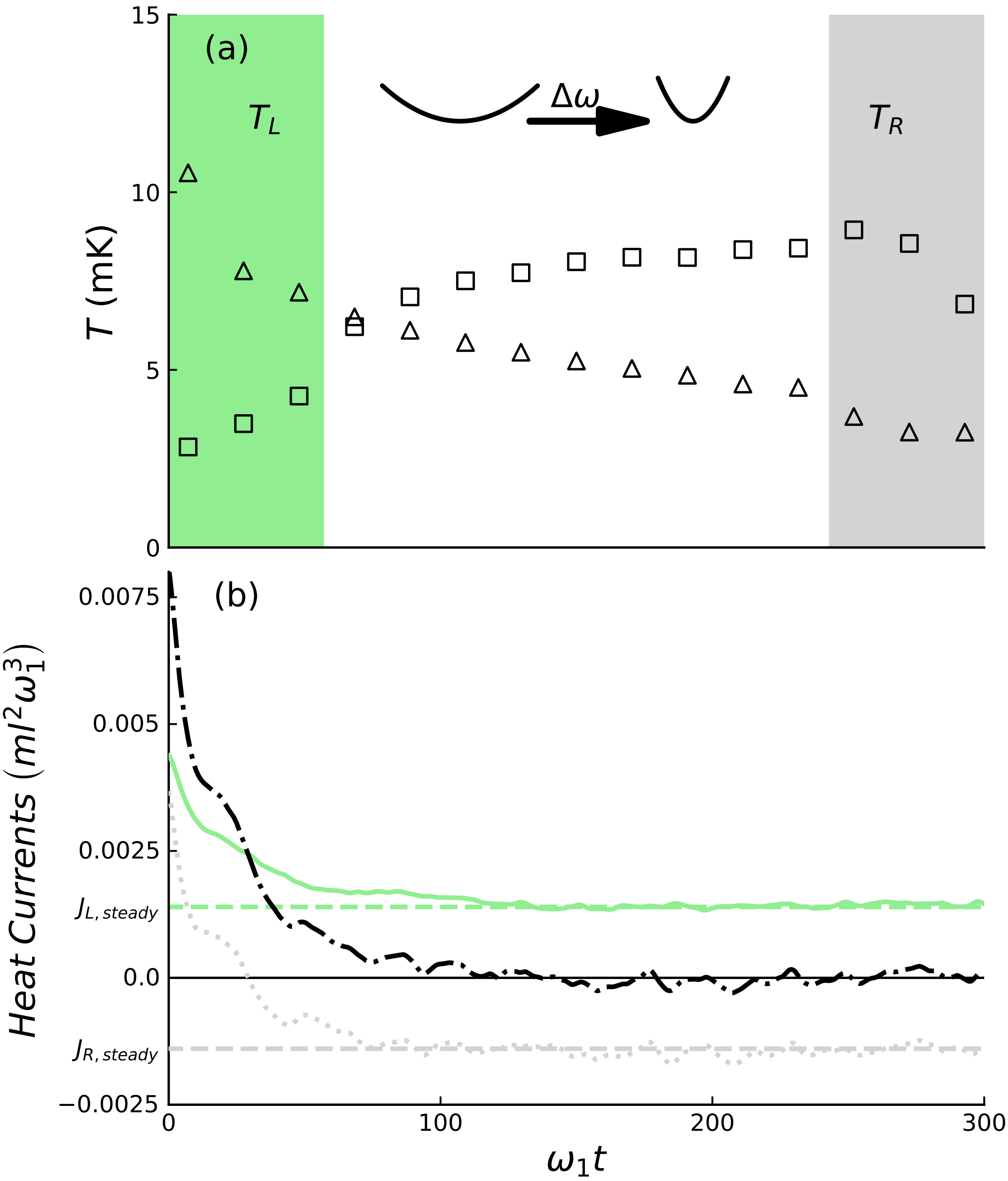

FIGURE 1.2: (a) Temperatures of the ions in the stationary state for a graded chain with the parameters described in section 1.4.1. The temperature profiles found with the algebraic method (Eq. (1.17)) are indistinguishable from the ones found solving the Langevin equation (Eq. (1.3)). Empty triangles (squares) correspond to $T_L = T_H$ ($T_L = T_C$) and $T_R = T_C$ ($T_R = T_H$). (b) Heat currents as a function of time for $T_L = T_H$ and $T_R = T_C$, see Eq. (1.9): $J_L(t)$ (solid green line) from the left reservoir into the chain; $J_R(t)$ (dotted grey line) from the right reservoir into the chain (negative except at very short times); $J_L(t) + J_R(t)$ (dotted-dashed black line), which must go to zero in the steady state. The three lines tend to stationary values marked by horizontal lines. Parameters: $\omega_1 = 2\pi \times 50$ kHz, $a = 50\,\mu$m, $\delta_H = -0.02\,\Gamma$, and $\delta_C = -0.1\,\Gamma$, which gives temperatures $T_H \approx 12$ mK and $T_C \approx 3$ mK. $\Delta\omega = 0.5\,\omega_1$. In all figures $\Gamma = 2\pi \times 41.3$ MHz.

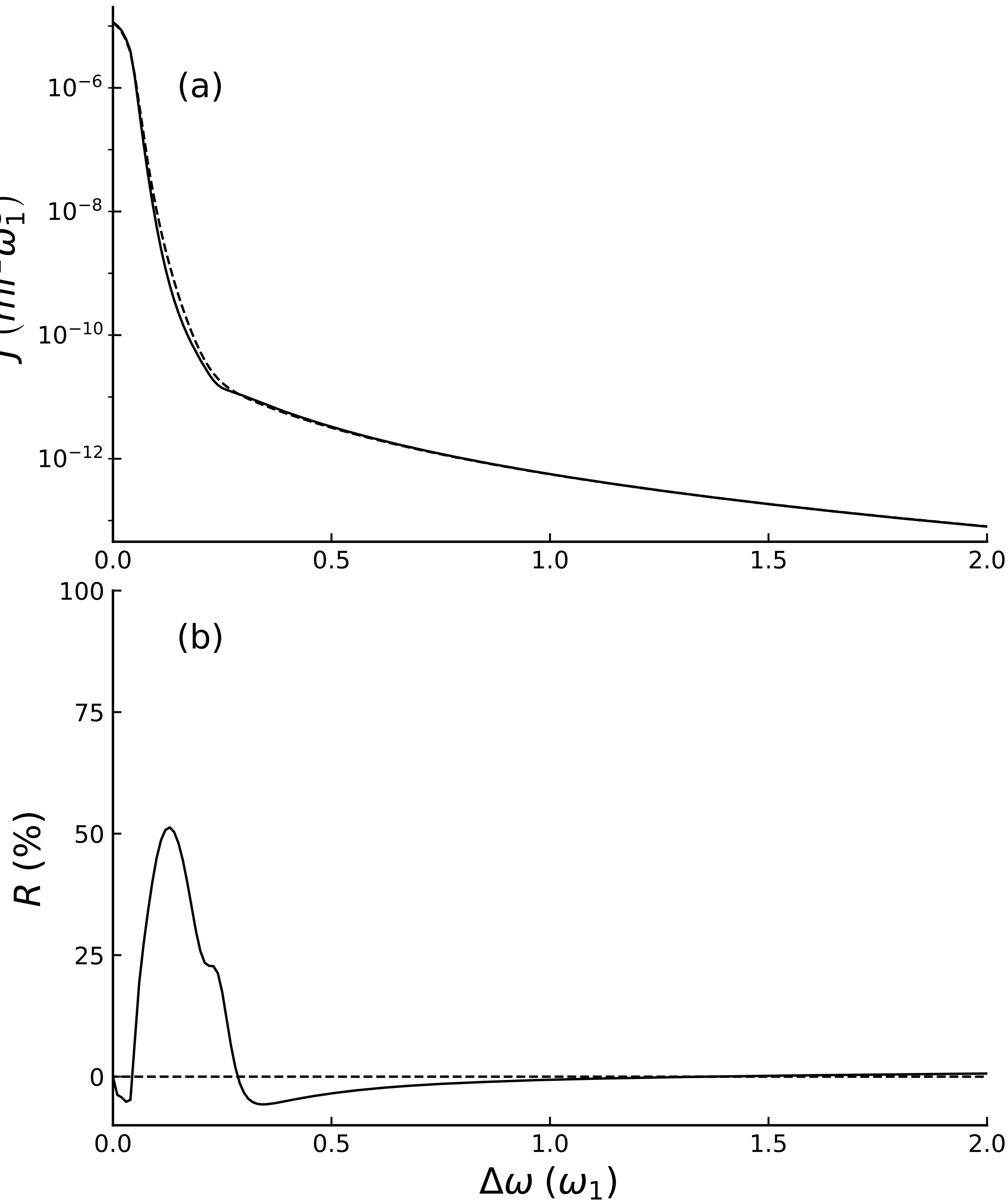

FIGURE 1.3: Graded chain of $N = 15$ $^{24}\mathrm{Mg}^{+}$ ions. (a) Stationary fluxes for different frequency increments: $J_{\rightarrow}$ (for $T_L = T_H$ and $T_R = T_C$, dashed line); $J_{\leftarrow}$ (for $T_L = T_C$ and $T_R = T_H$, solid line) (b) Rectification factor. Parameters: $\omega_1 = 2\pi \times 1$ MHz, $l = 5.25$ μm, $a = 4.76\,l$ ($25\,\mu$m), $\delta_H = -0.02\,\Gamma$, and $\delta_C = -0.1\,\Gamma$.

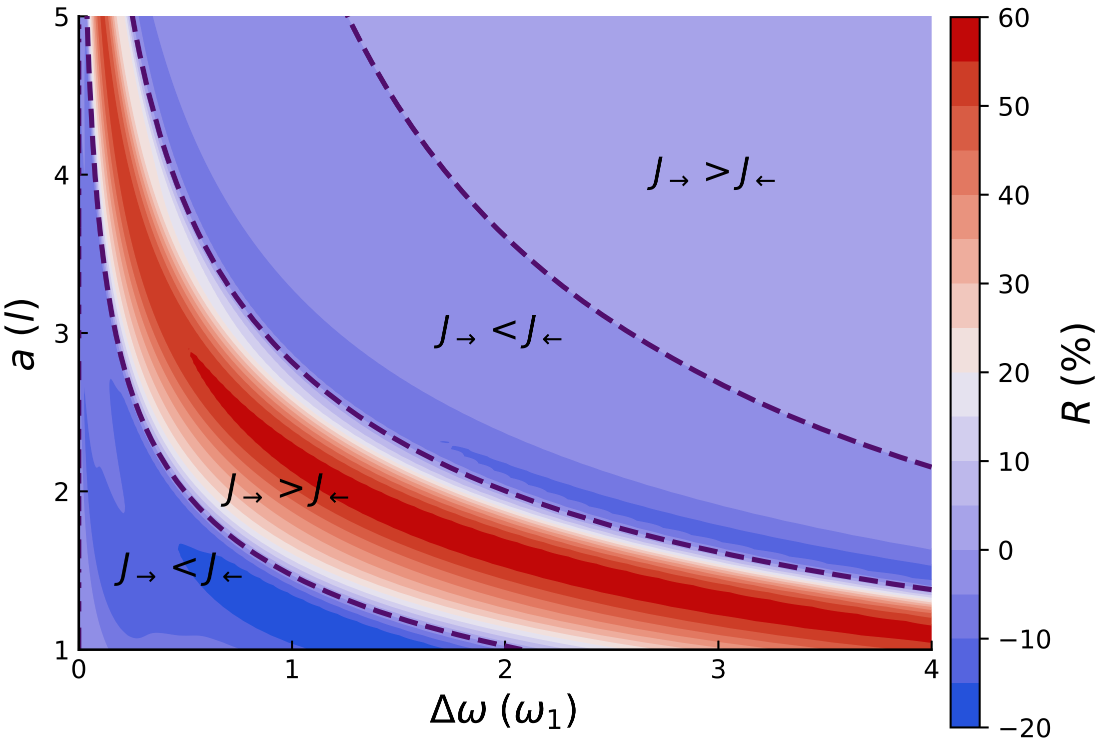

FIGURE 1.4: Rectification factor in a graded chain of $N = 15$ $^{24}Mg^+$ ions for different trap distances and frequency increment. The dashed lines are for $R = 0$ and delimit the regions $J_\rightarrow > J_\leftarrow$ and $J_\rightarrow < J_\leftarrow$. The parameters are $\omega_1 = 2\pi \times 1$ MHz, $l = 5.25\,\mu$m, $\delta_H = -0.02\,\Gamma$, and $\delta_C = -0.1\,\Gamma$.

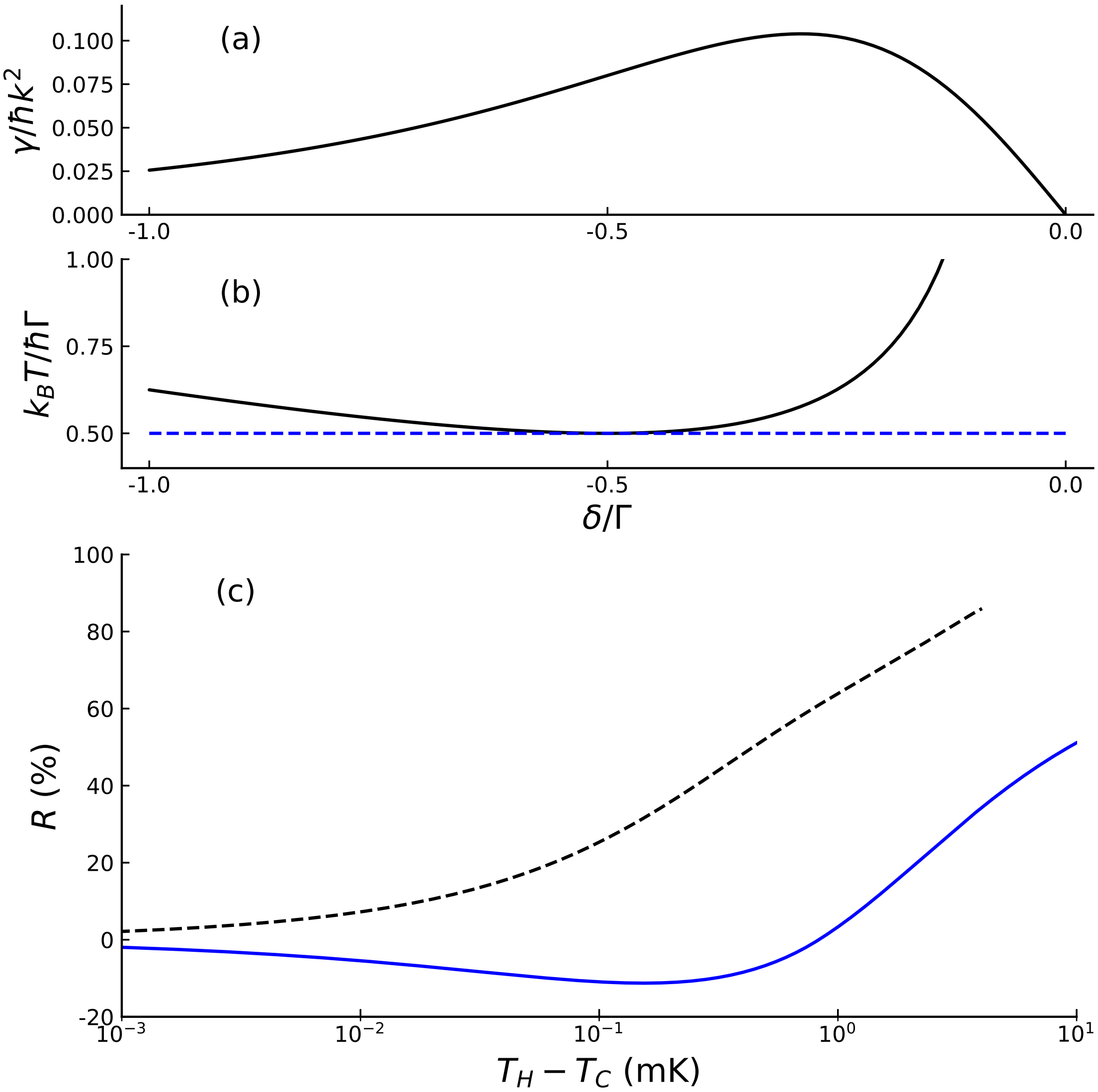

FIGURE 1.5: (a) Friction coefficient defined in Eq. (1.4). (b) Bath temperature defined in Eq. (1.5). (c) Rectification as a function of the temperature difference between the hot and cold baths $T_H - T_C$ for δ_H below (dashed black line) and above (solid blue line) the Doppler limit, and $\delta_C = \delta_D$ (Doppler limit). Parameters: $\omega_1 = 2\pi \times 1$ MHz, $\Delta\omega = 0.15\,\omega_1$, $l = 5.25\,\mu$m, $a = 4.76\,l$.

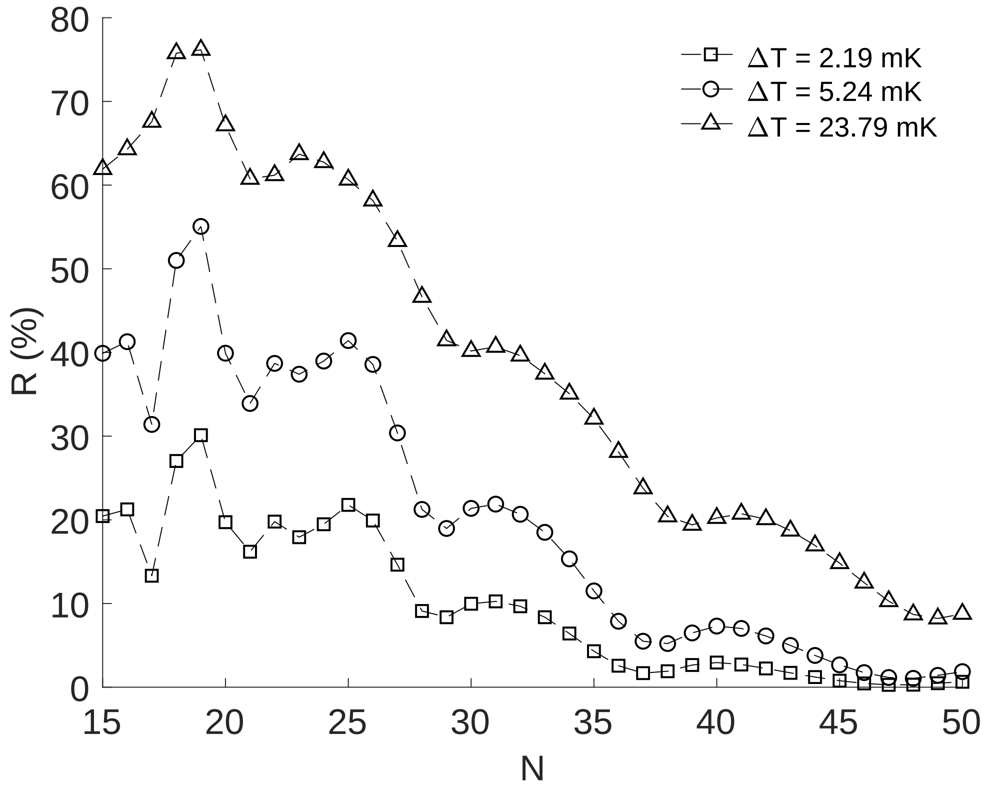

FIGURE 1.6: Rectification factor for different bath temperature differences ΔT as the number of ions is increased. The detuning of the cold bath laser is set to the Doppler limit $\delta_C = -\Gamma/2$. $\omega_1 = 2\pi \times 1$ MHz, $\Delta\omega = 0.15\,\omega_1$, $l = 5.25\,\mu$m, $a = 4.76\,l$.

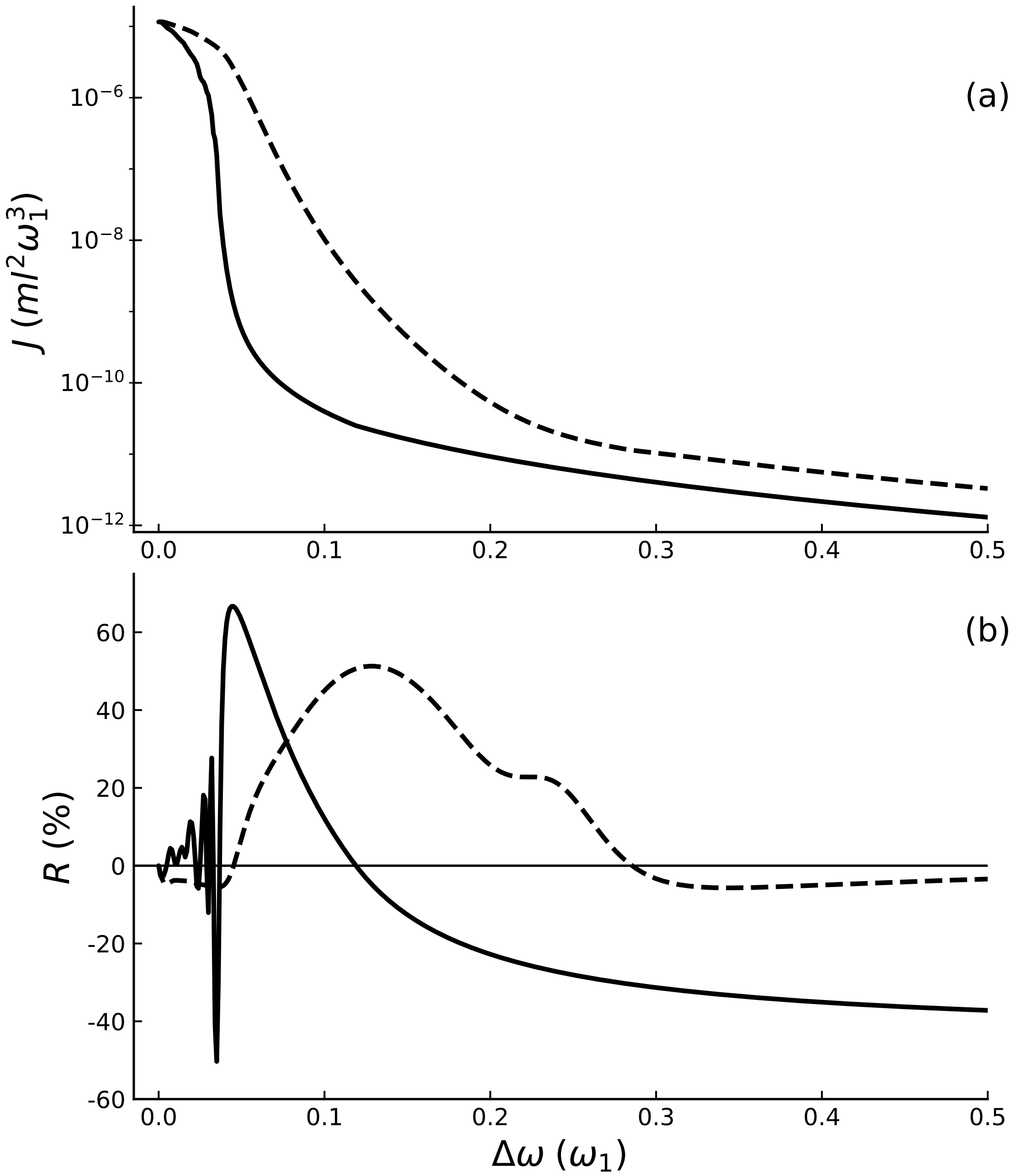

FIGURE 1.7: Comparison of graded and segmented chains with $N = 15$ $^{24}\mathrm{Mg}^+$ ions. (a) Maximum of $J_{\rightarrow}$ and $J_{\leftarrow}$ for the graded and segmented chain for different frequency increments. (b) Rectification factor: graded chain (dashed lines); segmented chain (solid lines). Parameters: $\omega_1 = 2\pi \times 1$ MHz, $l = 5.25\,\mu$m, $a = 4.76\,l$, $\delta_H = -0.02\,\Gamma$, and $\delta_C = -0.1\,\Gamma$.

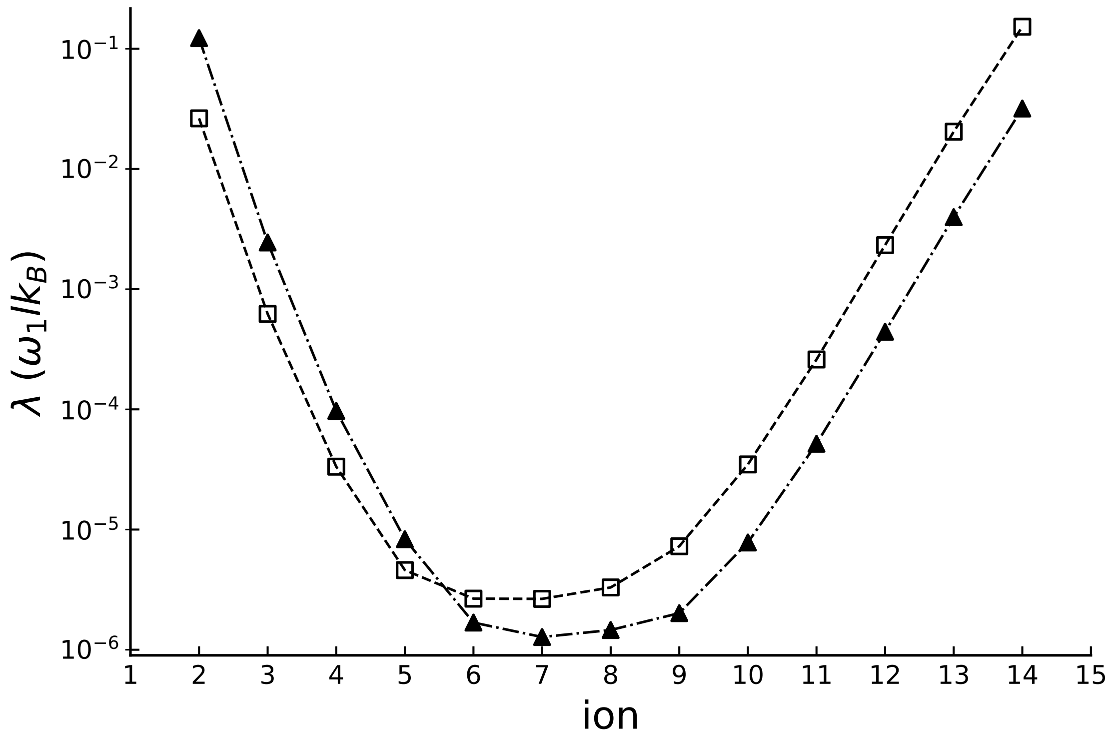

FIGURE 1.8: Thermal conductivity through the chain for $T_L > T_R$ (empty squares), and $T_L < T_R$ (filled triangles). $\omega_1 = 2\pi \times 1$ MHz, $\Delta\omega = 0.15\,\omega_1$, $l = 5.25\,\mu$m, $a = 4.76\,l$, $\delta_H = -0.02\,\Gamma$ and $\delta_C = -0.1\,\Gamma$.

Chapter 2

Rectification in a toy model

We study heat rectification in a minimalistic model composed of two masses subjected to on-site and coupling linear forces in contact with effective Langevin baths induced by laser interactions. Analytic expressions of the heat currents in the steady state are spelled out. Asymmetric heat transport is found in this linear system if both the bath temperatures and the temperature dependent bath-system couplings are also exchanged.

2.1 Introduction

Heat rectification, firstly observed in 1936 by Starr [1], is the physical phenomenon, analogous to electrical current rectification in diodes, in which heat current through a device or medium is not symmetric with respect to the exchange of the baths at the boundaries. In the limiting case the device allows heat to propagate in one direction from the hot to the cold bath while it behaves as a thermal insulator in the opposite direction when the baths are exchanged. In 2002 a paper by Terraneo *et al.* [2] demonstrated heat rectification numerically for a chain of nonlinear oscillators in contact with two thermal baths at different temperatures. Since then, there has been a growing interest in heat rectification [3–14, 22, 67], and the field remains very active because of the potential applications in fundamental science and technology, and the fact that none of the proposals so far appears to be efficient and robust for practical purposes.

Much effort has been devoted to understand the underlying physical mechanism responsible for rectification [3]. In early times some kind of anharmonicity, i.e. non-linear forces, in the substrate potential or in the particle-particle interactions, was identified as a fundamental requisite for rectification [5, 15–19]. This non-harmonic behavior leads to a temperature dependence of the phonon bands. The match/mismatch of the phonon bands (power spectra) governs the heat transport in the chain, allowing it when the bands match or obstructing it if they mismatch [2, 20]. However, a work by Pereira *et al.* [21] showed that rectification can also be found in effective harmonic systems if two requirements are met: some kind of structural asymmetry, and features that depend on the temperature so they change as the baths are inverted. Indeed, in this article we demonstrate rectification in a minimalistic model of two harmonic oscillators where the coupling to the baths depends on the temperature. This will be justified with a particular physical set up with trapped ions and lasers.

The article is organized as follows. In Section 2.2 we describe the physical model and its dynamical equations. In Section 2.3 we describe the dynamics of the system in terms of a covariance matrix. We also derive a set of algebraic equations that gives as solution the covariance matrix in the steady state. In Section 2.4 we solve the covariance matrix equations and find analytical expressions for the steady-state temperatures of the masses and heat currents. In Section 2.5 we relate the parameters of our model to those in a physical set-up of Doppler cooled trapped

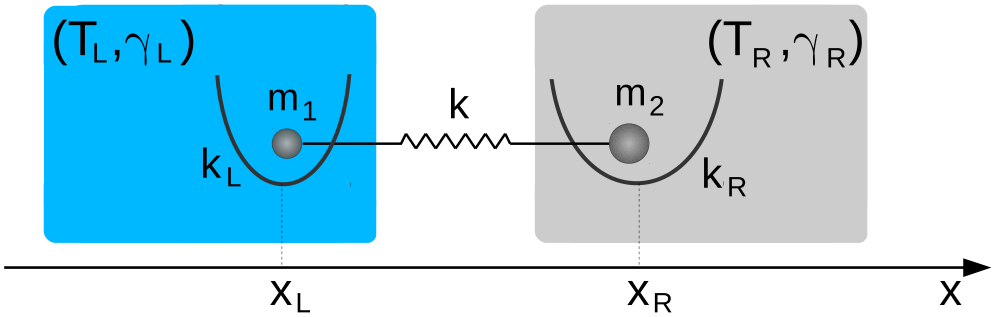

FIGURE 2.1: Diagram of the model described in Section 2.2. Two ions coupled to each other through a spring constant k. Each ion is harmonically trapped and connected to a bath characterized by its temperature T_i and its friction coefficient γ_i.

ions. In Section 2.6 we make a parameter sweep looking for configurations which yield high rectification. We also study the power spectra of the oscillators, which confirm the match/mismatch patterns in cases where there is rectification. In Section 2.7 we summarize our results and present our conclusions.

2.2 Physical Model

The physical model consists of two masses m_1 and m_2 coupled to each other by a harmonic interaction with spring constant k and natural length x_e. Each of the masses m_1 and m_2 are confined by a harmonic potential with spring constants k_L, k_R and equilibrium positions x_L, x_R respectively (see Fig. 2.1). The Hamiltonian describing this model is

$$H = \frac{p_1^2}{2m_1} + \frac{p_2^2}{2m_2} + V(x_1, x_2), \tag{2.1}$$

with $V(x_1, x_2) = \frac{k}{2}(x_1 - x_2 - x_e)^2 + \frac{k_L}{2}(x_1 - x_L)^2 + \frac{k_R}{2}(x_2 - x_R)^2$, where $\{x_i, p_i\}_{i=1,2}$ are the position and momentum of each mass. Switching from the original coordinates x_i to displacements with respect to the equilibrium positions of the system $q_i = x_i - x_i^{eq}$, where x_i^{eq} are the solutions to $\partial_{x_i} V(x_1, x_2) = 0$, the Hamiltonian can be written as

$$
\begin{aligned}
H = {} & \frac{p_1^2}{2m_1} + \frac{p_2^2}{2m_2} + \frac{k+k_L}{2} q_1^2 \\
& + \frac{k+k_R}{2} q_2^2 - k q_1 q_2 + V(x_1^{eq}, x_2^{eq}).
\end{aligned} \tag{2.2}
$$

This has the form of the Hamiltonian of a system around a stable equilibrium point

$$
H = \frac{1}{2} \overrightarrow{p}^{\mathsf{T}} \mathbb{M}^{-1} \overrightarrow{p} + \frac{1}{2} \overrightarrow{q}^{\mathsf{T}} \mathbb{K} \overrightarrow{q}, \tag{2.3}
$$

where $\overrightarrow{q} = (q_1, q_2)^{\mathsf{T}}$, $\overrightarrow{p} = (p_1, p_2)^{\mathsf{T}}$, $\mathbb{M} = diag(m_1, m_2)$ is the mass matrix of the system and $\mathbb{K}$ is the Hessian matrix of the potential at the equilibrium point, i.e., $\mathbb{K}_{ij} = \partial^2_{x_i, x_j} V(\overrightarrow{x})\Big|_{\overrightarrow{x} = \overrightarrow{x}^{eq}}$. In this model $\mathbb{K}_{11} = k + k_L$, $\mathbb{K}_{22} = k + k_R$ and $\mathbb{K}_{12} = \mathbb{K}_{21} = -k$. We shall see later that the generic form (2.3) can be adapted to different physical settings, in particular to two ions in individual traps, or to two ions in a common trap.

The masses are in contact with Langevin baths, which will be denoted as L (for left) and R (for right), at temperatures T_L and T_R for the mass m_1 and m_2 respectively (see Fig. 2.1). The equations of motion of the system, taking into account the Hamiltonian and the Langevin baths are

$$
\begin{aligned}
\dot{q}_1 &= \frac{p_1}{m_1}, \\
\dot{q}_2 &= \frac{p_2}{m_2}, \\
\dot{p}_1 &= -(k + k_L) q_1 + k q_2 - \frac{\gamma_L}{m_1} p_1 + \xi_L(t), \\
\dot{p}_2 &= -(k + k_R) q_2 + k q_1 - \frac{\gamma_R}{m_2} p_2 + \xi_R(t),
\end{aligned} \tag{2.4}
$$

where γ_L, γ_R are the friction coefficients of the baths and $\xi_L(t)$, $\xi_R(t)$ are Gaussian white-noise-like forces. The Gaussian forces have zero mean ($\langle \xi_L(t) \rangle = \langle \xi_R(t) \rangle = 0$) and satisfy the correlations $\langle \xi_L(t) \xi_R(t') \rangle = 0$, $\langle \xi_L(t) \xi_L(t') \rangle = 2D_L \delta(t - t')$, $\langle \xi_R(t) \xi_R(t') \rangle = 2D_R \delta(t - t')$. D_L and D_R are the diffusion coefficients, which satisfy the fluctuation-dissipation theorem: $D_L = \gamma_L k_B T_L$, $D_R = \gamma_R k_B T_R$ (k_B is the Boltzmann constant).

It is useful to define the phase-space vector $\overrightarrow{r}(t) = (\overrightarrow{q}, \mathbb{M}^{-1}\overrightarrow{p})^{\mathsf{T}}$ (note that $\overrightarrow{v} = \mathbb{M}^{-1}\overrightarrow{p}$ is just the velocity vector) so the equations of motion for this vector are

$$\dot{\vec{r}}(t) = \mathbb{A}\,\vec{r}(t) + \mathbb{L}\,\vec{\xi}(t), \tag{2.5}$$

with

$$\begin{aligned} \mathbb{A} &= \begin{pmatrix} \nvdash_{2\times 2} & \nVdash_{2\times 2} \\ -\mathbb{M}^{-1}\mathbb{K} & -\mathbb{M}^{-1}\Gamma \end{pmatrix}, \\ \mathbb{L} &= \begin{pmatrix} \nvdash_{2\times 2} \\ \mathbb{M}^{-1} \end{pmatrix}, \end{aligned} \tag{2.6}$$

and $\vec{\xi}(t) = (\xi_L(t), \xi_R(t))^{\mathsf{T}}$, $\Gamma = diag(\gamma_L, \gamma_R)$. $\nvdash_{n\times n}$ and $\nVdash_{n\times n}$ are the n-th dimensional squared 0 matrix and identity matrix respectively. With the vector notation the correlation of the white-noise forces can be written as

$$\left\langle \vec{\xi}(t)\,\vec{\xi}(t')^{\mathsf{T}} \right\rangle = 2\mathbb{D}\delta(t - t'), \tag{2.7}$$

with $\mathbb{D} = diag(D_L, D_R)$.

2.3 Covariance matrix in the steady state

We define the covariance matrix of the system as $\mathbb{C}(t) = \langle \vec{r}(t)\vec{r}(t)^{\mathsf{T}} \rangle$. This matrix is important because the heat transport properties can be extracted from it. In particular, the kinetic temperatures of the masses, $T_1(t)$ and $T_2(t)$, are

$$\begin{aligned} T_1(t) &= \frac{\langle p_1^2(t) \rangle}{m_1 k_B} = \frac{m_1 C_{3,3}(t)}{k_B}, \\ T_2(t) &= \frac{\langle p_2^2(t) \rangle}{m_2 k_B} = \frac{m_2 C_{4,4}(t)}{k_B}. \end{aligned} \tag{2.8}$$

One approach to find the covariance matrix is to solve Eq. (2.5). However, this requires solving the equations explicitly or simulate them numerically many times to find the covariance matrix for the ensemble of simulated stochastic trajectories. Instead, we proceed by looking for an ordinary differential equation that gives the evolution of the covariance matrix as described in [53, 68, 69]. Differentiating $\mathbb{C}(t)$

with respect to time and using Eq. (2.5) we get

$$\begin{aligned}\frac{d}{dt}\mathbb{C}(t) &= \mathbb{A}\mathbb{C}(t) + \mathbb{C}(t)\mathbb{A}^{\mathsf{T}} \\ &+ \mathbb{L}\left\langle \overrightarrow{\xi}(t)\overrightarrow{r}(t)^{\mathsf{T}}\right\rangle \\ &+ \left\langle \overrightarrow{r}(t)\overrightarrow{\xi}(t)^{\mathsf{T}}\right\rangle \mathbb{L}^{\mathsf{T}}.\end{aligned} \tag{2.9}$$

The solution of Eq. (2.9) allows us to find the local temperatures of the masses as a function of the bath temperatures (Eq. (2.8)) at all times. In particular, we are interested in the covariance matrix in the steady state, i.e., for $t \to \infty$. According to the Novikov Theorem [49] we can write down the covariance matrix in the steady state without having to integrate the differential equation. We now show how to get the steady-state covariance matrix.

In the steady state, the covariance matrix is constant ($\frac{d}{dt}\mathbb{C}(t) = 0$), therefore it satisfies

$$\begin{aligned}&\mathbb{A}\mathbb{C}^{s.s.} + \mathbb{C}^{s.s.}\mathbb{A}^{\mathsf{T}} = \\ &-\mathbb{L}\left\langle \overrightarrow{\xi}\overrightarrow{r}^{\mathsf{T}}\right\rangle^{s.s.} - \left\langle \overrightarrow{r}\overrightarrow{\xi}^{\mathsf{T}}\right\rangle^{s.s.}\mathbb{L}^{\mathsf{T}},\end{aligned} \tag{2.10}$$

with $\{\cdot\}^{s.s.} \equiv \lim_{t\to\infty}\{\cdot\}(t)$. Equation (2.10) is an algebraic equation whose solution is the steady-state covariance matrix $\mathbb{C}^{s.s.}$. However, the two terms $\left\langle \overrightarrow{\xi}\overrightarrow{r}^{\mathsf{T}}\right\rangle^{s.s.}$ and $\left\langle \overrightarrow{r}\overrightarrow{\xi}^{\mathsf{T}}\right\rangle^{s.s.}$ need to be calculated before working out the solution. One approach to calculate $\left\langle \overrightarrow{\xi}\overrightarrow{r}^{\mathsf{T}}\right\rangle^{s.s.}$ would be to solve Eq. (2.5), but this is exactly what we are trying to avoid. It is here when the Novikov theorem comes useful, since it lets us compute $\left\langle \overrightarrow{\xi}\overrightarrow{r}^{\mathsf{T}}\right\rangle^{s.s.}$ without having to integrate the equations of motion. Using this theorem and the δ-correlation of the noises, we find the ij-th component of $\left\langle \overrightarrow{\xi}(t)\overrightarrow{r}(t)^{\mathsf{T}}\right\rangle$,

$$\begin{aligned}\langle \xi_i(t) r_j(t)\rangle &= \sum_{k=1}^{2}\int_0^t d\tau\ \langle \xi_i(t)\xi_k(\tau)\rangle \left\langle \frac{\delta r_j(t)}{\delta\xi_k(\tau)}\right\rangle \\ &= \sum_{k=1}^{2}\mathbb{D}_{ik}\lim_{\tau\to t^-}\left\langle \frac{\delta r_j(t)}{\delta\xi_k(\tau)}\right\rangle,\end{aligned} \tag{2.11}$$

where $\lim\limits_{\tau\to t^-}$ is the limit when τ goes to t from below. Evaluation of the functional derivative $\delta r_j(t)/\delta\xi_k(\tau)$ for the $\tau \to t^-$ limit gives

$$\left\langle \overrightarrow{\xi}(t)\overrightarrow{r}(t)^{\mathsf{T}} \right\rangle = \mathbb{D}\mathbb{L}^{\mathsf{T}}. \tag{2.12}$$

Now, the algebraic equation that gives the steady-state covariance matrix becomes

$$\mathbb{A}\mathbb{C}^{s.s.} + \mathbb{C}^{s.s.}\mathbb{A}^{\mathsf{T}} = -\mathbb{B}, \tag{2.13}$$

with $\mathbb{B} = 2\mathbb{L}\mathbb{D}\mathbb{L}^{\mathsf{T}}$. By definition, the covariance matrix is symmetric, but there are also additional restrictions imposed by the equations of motion and the steady-state condition, which reduce the dimensionality of the problem of solving Eq. (2.13) [70]. Since $d\langle q_i q_j\rangle/dt = 0$ in the steady state, we have

$$\begin{aligned} \langle p_1 q_1\rangle^{s.s.} &= \langle p_2 q_2\rangle^{s.s.} = 0, \\ \frac{\langle p_1 q_2\rangle^{s.s.}}{m_1} &= -\frac{\langle q_1 p_2\rangle^{s.s.}}{m_2}. \end{aligned} \tag{2.14}$$

Taking (2.14) into account, the steady-state covariance matrix takes the form

$$\mathbb{C}^{s.s.} = \begin{pmatrix} \langle q_1^2\rangle^{s.s.} & \langle q_1 q_2\rangle^{s.s.} & 0 & \frac{\langle p_2 q_1\rangle^{s.s.}}{m_2} \\ \langle q_1 q_2\rangle^{s.s.} & \langle q_2^2\rangle^{s.s.} & -\frac{\langle p_2 q_1\rangle^{s.s.}}{m_2} & 0 \\ 0 & -\frac{\langle p_2 q_1\rangle^{s.s.}}{m_2} & \frac{\langle p_1^2\rangle^{s.s.}}{m_1^2} & \frac{\langle p_1 p_2\rangle^{s.s.}}{m_1 m_2} \\ \frac{\langle p_2 q_1\rangle^{s.s.}}{m_2} & 0 & \frac{\langle p_1 p_2\rangle^{s.s.}}{m_1 m_2} & \frac{\langle p_2^2\rangle^{s.s.}}{m_2^2} \end{pmatrix}. \tag{2.15}$$

The explicit set of equations for the components of $\mathbb{C}^{s.s}$ can be found in Appendix .1.

2.4 Solutions

In this section we use the solution to Eq. (2.13) to write down the temperatures and currents in the steady state. We use Mathematica to obtain analytic expressions for the temperatures,

$$\begin{aligned} T_1 &= \frac{T_L\mathcal{P}_{1,L}(k) + T_R\mathcal{P}_{1,R}(k)}{\mathcal{D}(k)}, \\ T_2 &= \frac{T_L\mathcal{P}_{2,L}(k) + T_R\mathcal{P}_{2,R}(k)}{\mathcal{D}(k)}, \end{aligned} \tag{2.16}$$

where $\mathcal{D}(k) = \sum_{n=0}^{2} \mathcal{D}_n k^n$ and $\mathcal{P}_{i,(L/R)}(k) = \sum_{n=0}^{2} a_{i,n,(L/R)} k^n$ are polynomials in the coupling constant k with coefficients

$$\begin{aligned}
\mathcal{D}_0 &= a_{1,0,L} = a_{2,0,R} = \gamma_L \gamma_R \left[h^{(1)} \left(\gamma_L k_R + \gamma_R k_L \right) + \left(m_1 k_R - m_2 k_L \right)^2 \right], \\
\mathcal{D}_1 &= a_{1,1,L} = a_{2,1,R} = \gamma_L \gamma_R \left[h^{(0)} h^{(1)} + 2 \left(m_1 - m_2 \right) \left(m_1 k_R - m_2 k_L \right) \right], \\
\mathcal{D}_2 &= h^{(0)} h^{(2)}, \\
a_{1,2,L} &= \gamma_L \left(m_2 h^{(1)} + \gamma_R (m_1 - m_2)^2 \right), \\
a_{1,2,R} &= h^{(1)} m_1 \gamma_R, \\
a_{2,2,L} &= h^{(1)} m_2 \gamma_L, \\
a_{2,2,R} &= \gamma_R \left(m_1 h^{(1)} + \gamma_L (m_1 - m_2)^2 \right), \\
a_{1,0,R} &= a_{1,1,R} = a_{2,0,L} = a_{2,1,L} = 0,
\end{aligned} \tag{2.17}$$

where $h^{(n)} \equiv \gamma_R m_1^n + \gamma_L m_2^n$. The currents from the baths to the masses [70] are

$$\begin{aligned}
J_L &= k_B \frac{\gamma_L}{m_1} \left(T_L - T_1 \right), \\
J_R &= k_B \frac{\gamma_R}{m_2} \left(T_R - T_2 \right),
\end{aligned} \tag{2.18}$$

with T_i given by Eq. (2.16). Since, in the steady state, $J_L = -J_R$ we will use the shorthand notation $J \equiv J_L$. Substituting Eq. (2.16) into Eq. (2.18) we get for the heat current

$$J = \kappa \left(T_L - T_R \right), \tag{2.19}$$

where $\kappa = k_B k^2 \gamma_L \gamma_R h^{(1)} / \mathcal{D}(k)$ acts as an effective thermal conductance, which depends on the parameters of the system, i.e., the masses and spring constants, and also on the friction coefficients of the baths. From Eq. (2.19) it could be thought that inverting the temperatures of the baths would only lead to an exchange of heat currents. However, since the thermal conductance κ depends on the friction coefficients, the exchange of the baths implies a change in its value. Moreover, it is possible to have temperature-dependent friction coefficients, as it happens in the physical set-up of laser-cooled trapped ions described in Section 2.5.

2.5 Relation of the Model to a trapped ion set-up

As we mentioned, the parameters k, k_L and k_R can be related to the elements of the Hessian matrix of a system in a stable equilibrium position. In this section we will identify these parameters with the Hessian matrix of a pair of trapped ions. Here we consider two different set-ups: two ions in a collective trap, and two ions in individual traps. In Section 2.6 we focus on two ions in individual traps to illustrate the analysis of rectification.

In both set-ups we assume strong confinement in the radial direction, making the effective dynamics one-dimensional. We will also assume that the confinement in the axial direction is purely electrostatic, which makes the effective spring constant independent of the mass of the ions [71]. Additionally, we will relate the temperatures and friction coefficients of the Langevin baths to those corresponding to Doppler cooling.

2.5.1 Collective trap

Consider two ions of unit charge with masses m_1 and m_2 trapped in a collective trap. Assuming strong radial confinement and purely electrostatic axial confinement, both ions feel the same harmonic oscillator potential with trapping constant k_{trap} [71]. The potential describing the system is

$$V_{collective} = \frac{1}{2}k_{trap}\left(x_1^2 + x_2^2\right) + \frac{\mathcal{C}}{x_2 - x_1}, \tag{2.20}$$

with $\mathcal{C} = \frac{Q^2}{4\pi\varepsilon_0}$. The equilibrium positions for this potential are

$$x_2^{eq} = -x_1^{eq} = \left(\frac{1}{2}\right)^{2/3}\left(\frac{Q^2}{4\pi\varepsilon_0 k_{trap}}\right)^{1/3}. \tag{2.21}$$

Assuming small oscillations of the ions around the equilibrium positions, the Hessian matrix of the system is

$$
\begin{aligned}
\mathbb{K}_{1,2} &= -\frac{Q^2}{2\pi\varepsilon_0}\frac{1}{(x_2^{eq}-x_1^{eq})^3} = -k_{trap}, \\
\mathbb{K}_{1,1} &= k_{trap} + \frac{Q^2}{2\pi\varepsilon_0}\frac{1}{(x_2^{eq}-x_1^{eq})^3} = 2k_{trap}, \\
\mathbb{K}_{2,2} &= k_{trap} + \frac{Q^2}{2\pi\varepsilon_0}\frac{1}{(x_2^{eq}-x_1^{eq})^3} = 2k_{trap}.
\end{aligned} \tag{2.22}
$$

Using Eq. (2.22) we can relate the parameters of this physical set-up to those of the model described in Section 2.2 to find

$$k_L = k_R = k = k_{trap}. \tag{2.23}$$

2.5.2 Individual on-site traps

We can make the same assumptions for the axial confinement as in the previous subsection but now each of the ions is in an individual trap with spring constants $k_{trap,L}$ and $k_{trap,R}$ respectively. The potential of the system is

$$
\begin{aligned}
V_{individual} = &\frac{1}{2}k_{trap,L}\left(x_1 - x_L\right)^2 + \frac{1}{2}k_{trap,R}\left(x_2 - x_R\right)^2 \\
&+ \frac{\mathcal{C}}{x_2 - x_1},
\end{aligned} \tag{2.24}
$$

where x_L and x_R are the center positions of the on-site traps. The elements of the Hessian matrix in the equilibrium position are

$$
\begin{aligned}
\mathbb{K}_{1,2} &= -\frac{Q^2}{2\pi\varepsilon_0}\frac{1}{(x_2^{eq}-x_1^{eq})^3}, \\
\mathbb{K}_{1,1} &= k_{trap,L} + \frac{Q^2}{2\pi\varepsilon_0}\frac{1}{(x_2^{eq}-x_1^{eq})^3}, \\
\mathbb{K}_{2,2} &= k_{trap,R} + \frac{Q^2}{2\pi\varepsilon_0}\frac{1}{(x_2^{eq}-x_1^{eq})^3}.
\end{aligned} \tag{2.25}
$$

Comparing the parameters in Eq. (2.25) with those in the model described in Section 2.2 we identify

$$
\begin{aligned}
k_L &= k_{trap,L}, \\
k_R &= k_{trap,R}, \\
k &= \frac{Q^2}{2\pi\varepsilon_0}\frac{1}{(x_2^{eq}-x_1^{eq})^3}\,.
\end{aligned}
\tag{2.26}
$$

In this case, the analytic expressions for the equilibrium positions are more complicated. We get for the distance between the equilibrium positions of the ions

$$
\begin{aligned}
(x_2-x_1)^{(eq)} &= \frac{1}{3}\Delta x_{LR} \\
&- \frac{1}{6}\Big[\frac{2^{2/3}\zeta}{k_{trap,L}k_{trap,R}(k_{trap,L}+k_{trap,R})} \\
&+ \frac{2^{4/3}k_{trap,L}k_{trap,R}(k_{trap,L}+k_{trap,R})(x_R-x_L)^2}{\zeta}\Big]\,,
\end{aligned}
\tag{2.27}
$$

where $\Delta x_{LR} = (x_R - x_L)$ and $\zeta = (Y-\eta)^{(1/3)}$, with

$$
\begin{aligned}
Y &= 3\sqrt{3}\Big\{\mathcal{C}k_{trap,L}^4 k_{trap,R}^4\left(k_{trap,L}+k_{trap,R}\right)^7\times \\
&\quad \left[4k_{trap,L}k_{trap,R}\Delta x_{LR}^3 + 27\mathcal{C}\left(k_{trap,L}+k_{trap,R}\right)\right]\Big\}^{(1/2)}, \\
\eta &= k_{trap,L}^2 k_{trap,R}^2\left(k_{trap,L}+k_{trap,R}\right)^3\times \\
&\quad \left[2k_{trap,L}k_{trap,R}\Delta x_{LR}^3 + 27\mathcal{C}\left(k_{trap,L}+k_{trap,R}\right)\right]\,.
\end{aligned}
\tag{2.28}
$$

In this set-up, the coupling between the ions k can be controlled by changing the distance between the on-site traps.

2.5.3 Optical molasses and Langevin baths

Trapped ions may be cooled down by a pair of counterpropagating lasers which are red-detuned with respect to an internal atomic transition of the ions. This technique is known as Doppler cooling or optical molasses [46, 47, 72, 73]. The off-resonant absorption of laser photons by the ions exerts a damping-like force that slows them down. The spontaneous emission of the ions produces heating due to the random recoil generated by the emitted photons. Both, the friction and recoil force are in balance, and eventually the ion thermalizes to a finite temperature.

Thus the effect of the lasers on the ion is equivalent to a Langevin bath with temperature T_{molass} and friction coefficient γ_{molass}. The temperature and friction coefficients are controlled with the laser intensity I and frequency detuning δ with respect to the selected internal transition by the expressions [36, 46, 47],

$$\begin{aligned}\gamma_{molass}(I,\delta) &= -4\hbar\left(\frac{\delta+\omega_0}{c}\right)^2\left(\frac{I}{I_0}\right)\frac{2\delta/\Gamma}{[1+(2\delta/\Gamma)^2]^2},\\ T_{molass}(\delta) &= -\frac{\hbar\Gamma}{4k_B}\frac{1+(2\delta/\Gamma)^2}{(2\delta/\Gamma)},\end{aligned} \tag{2.29}$$

where ω_0 is the frequency of the selected internal atomic transition, Γ is the natural width of the excited state, and I_0 is the saturation intensity.

2.6 Looking for rectification

We will say that we observe rectification whenever the heat current J for a configuration of the baths changes when we exchange the baths to $\tilde{J}$. The important point here is to define what is meant by *exchanging the baths*. We consider that a bath is characterized, not only by its temperature T but also by its coupling to the system by means of the friction coefficient γ, so, exchanging the baths is achieved by exchanging both the temperatures and the friction coefficients, as summarized in Table 2.1.

When implementing temperatures and friction coefficients by lasers, this exchange operation is performed by changing the values of the intensities and detunings acting on each ion (Eq. (2.29)). The exchange operation is straightforward when the two ions are either of the same species or isotopes of each other, since the only required action is to exchange the values of the detunings of the lasers without modifying the intensities. However, if we deal with two different species, i.e., with two different atomic transitions, the laser wavelengths and the decay rates depend on the species. Then, exchanging the temperatures by modifying the detunings, keeping the laser intensities constant, does not necessarily imply an exchange of the friction coefficients. Nevertheless it is possible to adjust the laser intensities so that the friction coefficients get exchanged and that is the assumption hereafter. The idea of implementing a bath exchange like this follows the same line of thought as [21], since we are adding a temperature dependent feature to the system -the friction coefficients- that changes as the baths are inverted.

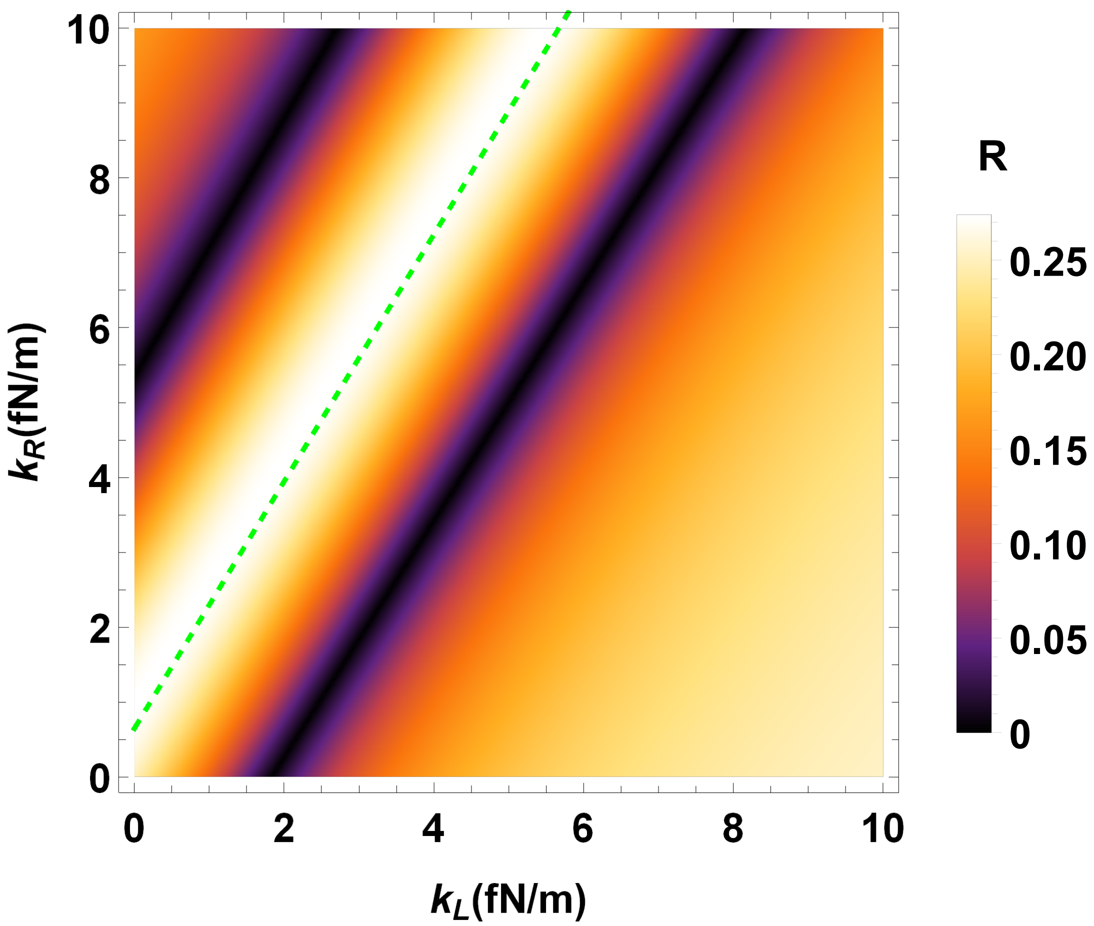

FIGURE 2.2: Rectification, R, in the $k_L k_R$ plane for $k = 1.17\times$ fN/m, $\gamma_L = 6.75 \times 10^{-22}$ kg/s, and $\gamma_R = 4.64\gamma_L$.

TABLE 2.1: Definition of forward and reversed (exchanged) bath configurations.

	forward	reversed
Bath Friction	γ_L, γ_R	$\tilde{\gamma}_L = \gamma_R$, $\tilde{\gamma}_R = \gamma_L$
Bath Temperature	T_L, T_R	$\tilde{T}_L = T_R$, $\tilde{T}_R = T_L$

To measure rectification, we will use the rectification coefficient R defined as

$$R = \frac{\left|J - \tilde{J}\right|}{\max(J, \tilde{J})}, \tag{2.30}$$

that is, the ratio between the difference of heat currents and the largest one. As defined, $R = 0$ for no asymmetry of the heat currents and $R = 1$ when they are maximally asymmetric.

2.6.1 Parametric exploration

We have explored thoroughly the space formed by the parameters of the model to find asymmetric heat transport, namely, $m_1, m_2, k, k_L, k_R, \gamma_L, \gamma_R$. We have fixed the values of some of the parameters to realistic ones while we have varied the rest. We have set the masses to $m_1 = 24.305$ a.u. and $m_2 = 40.078$ a.u., which correspond to Mg and Ca, whose ions are broadly used in trapped-ion physics. The temperatures are also fixed and, as Eq. (2.19) shows, rectification does not formally depend on the temperature in this model, unless we set the friction coefficients as a function of temperature using Eq. (2.29) explicitly.

Figure 2.2 depicts the values of the rectification after sweeping the $k_L k_R$ plane for fixed values of k, γ_L, and γ_R. A remarkable result from this figure is that parallel lines appear alternating minima and maxima of R. With a numerical fitting, we find that the line corresponding to the highest maximum value of R is determined by

$$\frac{k + k_L}{m_1} = \frac{k + k_R}{m_2}. \tag{2.31}$$

In a trapped-ion context the condition (2.31) may be imposed by adjusting the distance of the traps for fixed k_L and k_R. It is also remarkable that when Eq. (2.31) is satisfied, the rectification no longer depends on the spring constants of the model. This last result can be found assuming Eq. (2.31) when calculating the currents with Eq. (2.19) and R with Eq. (2.30),

$$R = \begin{cases} 1 - \frac{a+g}{1+ag} & \text{if } (a+g) < (1+ag) \\ 1 - \frac{1+ag}{a+g} & \text{if } (a+g) > (1+ag) \\ 0 & \text{if } (a+g) = (1+ag)\,, \end{cases} \tag{2.32}$$

where a and g are the mass and friction coefficients ratios

$$\begin{aligned} a &= m_2/m_1, \\ g &= \gamma_R/\gamma_L. \end{aligned} \tag{2.33}$$

The maximal rectification found does not scale with the magnitude of the masses or the friction coefficients, just with their ratios. Besides a high R, it is important to have non-vanishing heat currents [70]. Using again Eq. (2.31) in the expression for the currents (2.19), the maximum current $J_{\max} = \max(|J|, |\tilde{J}|)$ is

$$J_{\max} = \begin{cases} \frac{k_B g \gamma_L k^2 |T_L - T_R|}{(a+g)(g\gamma_L^2(k_L+k)+k^2 m_1)} & \text{if } (a+g) < (1+ag) \\ \frac{k_B g \gamma_L k^2 |T_L - T_R|}{(1+ag)(g\gamma_L^2(k_L+k)+k^2 m_1)} & \text{if } (a+g) > (1+ag)\,. \end{cases} \tag{2.34}$$

Now we analyze how the parameters a and g affect the maximum current J_{max} in (2.34). To do this, we can divide the ag plane in four quadrants by the axes $a = 1$ and $g = 1$ (in those axes $R = 0$). In Eq. (2.34) the parameter a appears only in the denominator, thus for a higher a, a smaller current is found. The quadrants with $a < 1$ will be better for achieving large currents. However, g appears both in the numerator and denominator so there is no obvious advantageous quadrant for this parameter.

Equation (2.32) is symmetric upon the transformations $a \leftrightarrow 1/a$ and $g \leftrightarrow 1/g$. Using a logarithmic scale for a and g, the resulting R map will be symmetric with respect to the $a = 1$ and $g = 1$ axes. We can limit ourselves to analyze the quadrant $a > 1$, $g > 1$, as the results in other quadrants will be equivalent upon transformations $a \leftrightarrow 1/a$ and $g \leftrightarrow 1/g$.

Fig. 2.3 shows the rectification given by Eq. (2.32) in terms of a and g. Along any diagonal line (parallel to the solid cyan or the dashed green lines), the maximum value is at the center, that is, when $a = g$. However, if we fix a, increasing g always increases R. Although we could increase g arbitrarily to get more rectification this is not a realistic option in a trapped-ion set-up. Since g is defined as the ratio between the friction coefficients, increasing it means making either γ_L go to 0 or γ_R to infinity. Making γ_L go to 0 decouples one of the ions from the bath, so the heat current tends to vanish in any direction. Also, increasing γ_R arbitrarily is impossible since the Doppler cooling friction coefficient as a function of the laser detuning (Eq. (2.29)) is bounded. Although Eq. (2.29) suggests that boosting the laser intensity can also increase the friction coefficient, this is not an option since Eq. (2.29) is just an approximation for low laser intensities. When going to higher intensities, the emission/absorption of photons by the ion is saturated and the friction coefficient reaches a finite value proportional to the width Γ of the excited state [47]. As a compromise between feasibility and high R, we set the ratio between the friction coefficients g to be equal to the mass ratio a. As shown in Fig. 2.3, along the solid-cyan and dashed-green diagonal lines the maximum R is achieved for $a = g$. Fig. 2.4 shows the rectification in Eq. (2.32)

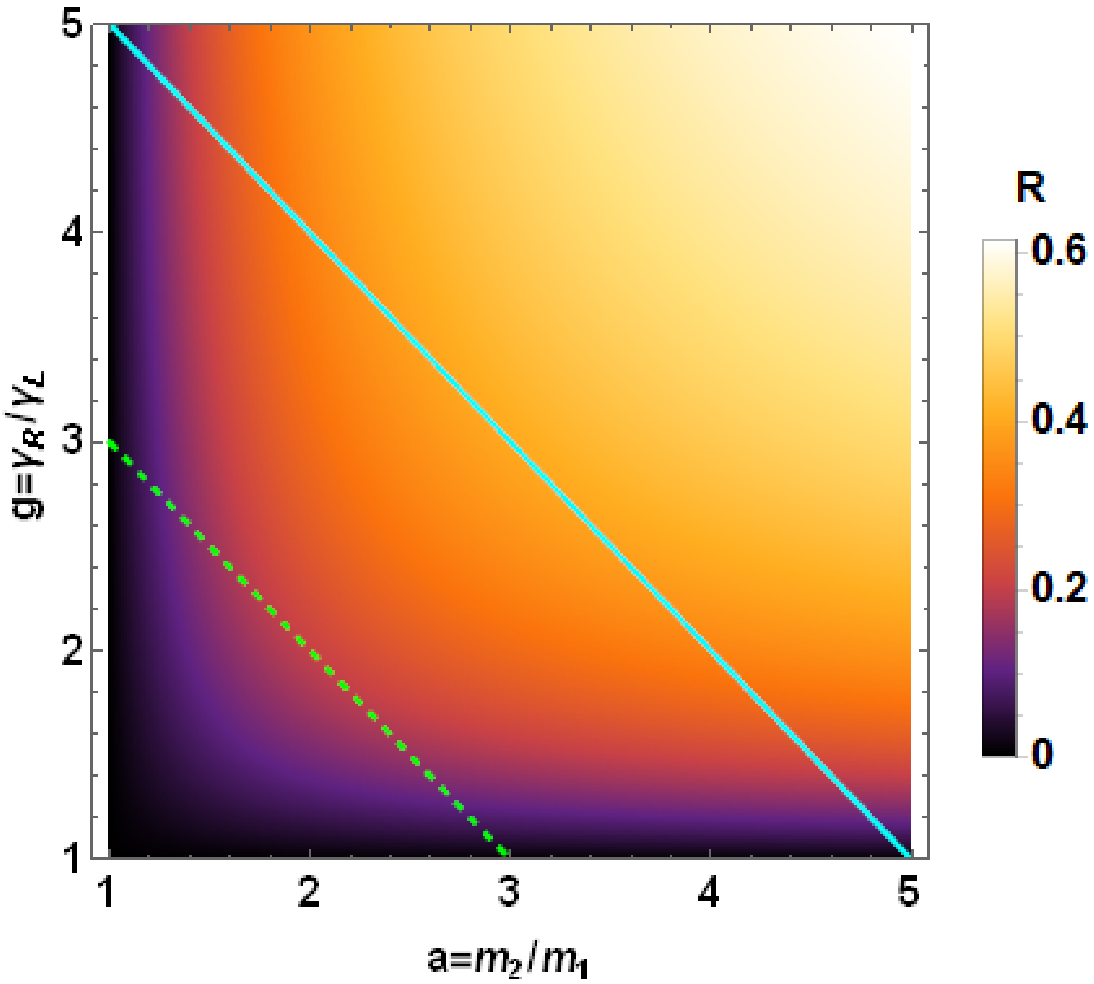

FIGURE 2.3: Rectification factor, R, given by Eq. (2.32).

for the line $a = g$. When both parameters are large enough, the rectification goes to 1.

2.6.2 Spectral match/mismatch approach to rectification

The match/mismatch between the power spectra of the particles controls the heat currents in the system [2, 20]. A good match between the power spectra of the two ions in a large range of frequencies yields a higher heat current through the system while the mismatch reduces the heat current. If there is a good match between the spectra of the ions (i.e., their peaks overlap in a broad range of frequencies) for a certain baths configuration, and mismatch when the baths exchange, the system will present heat rectification.

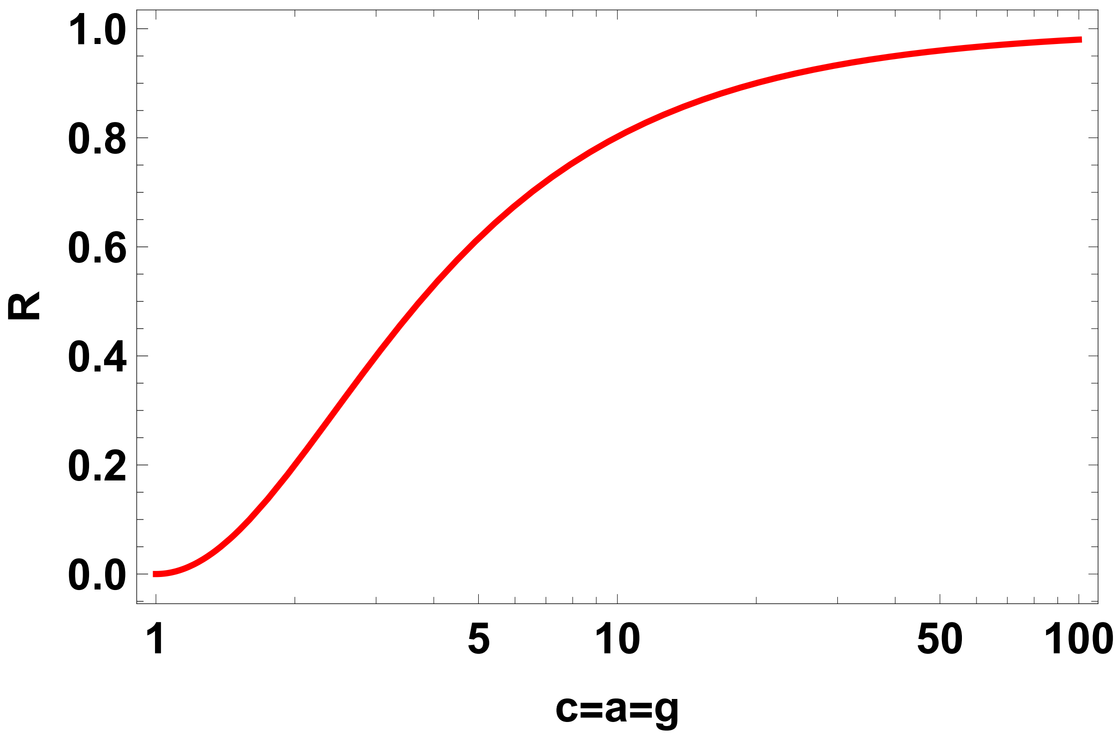

FIGURE 2.4: Rectification for different values of $c = m_2/m_1 = \gamma_R/\gamma_L$ when the maximum condition in the $k_L k_R$ plane is satisfied (Eq. (2.31)).

We have studied the phonon spectra of our model for several sets of parameters exhibiting no rectification or strong rectification. The phonon spectra of the ions is calculated through the spectral density matrix. For a real-valued stochastic process $\overrightarrow{x}(t)$, its spectral density matrix is defined as [53]

$$\mathbb{S}_{\overrightarrow{x}}(\omega) \equiv \left\langle \overrightarrow{X}(\omega)\overrightarrow{X}^{\mathsf{T}}(-\omega) \right\rangle, \tag{2.35}$$

with $\overrightarrow{X}(\omega)$ being the Fourier transform of $\overrightarrow{x}(t)$ (we are using the convention of multiplying by a factor of 1 and $\frac{1}{2\pi}$ for the transform and its inverse operation). A justification of the use of the spectral density matrix to understand heat transport arises from the Wiener-Khinchin theorem [53], which says that the correlation matrix of a stationary stochastic process in the steady state is the inverse Fourier transform of its spectral density matrix $\left\langle \overrightarrow{r}(t)\overrightarrow{r}^{\mathsf{T}}(t+\tau) \right\rangle = \mathcal{F}^{-1}[\mathbb{S}_{\overrightarrow{r}}(\omega)](\tau)$. This result allows us to write down the covariance matrix in the steady state through the spectral density as

$$\mathbb{C}^{s.s.} = \frac{1}{2\pi}\int_{-\infty}^{\infty} d\omega\; \mathbb{S}_{\overrightarrow{r}}(\omega). \tag{2.36}$$

Eq. (2.36) directly connects the spectral density matrix to the steady-state temperature and, therefore, to the heat currents (in Section 2.3 we saw that $T_1^{s.s.} =$

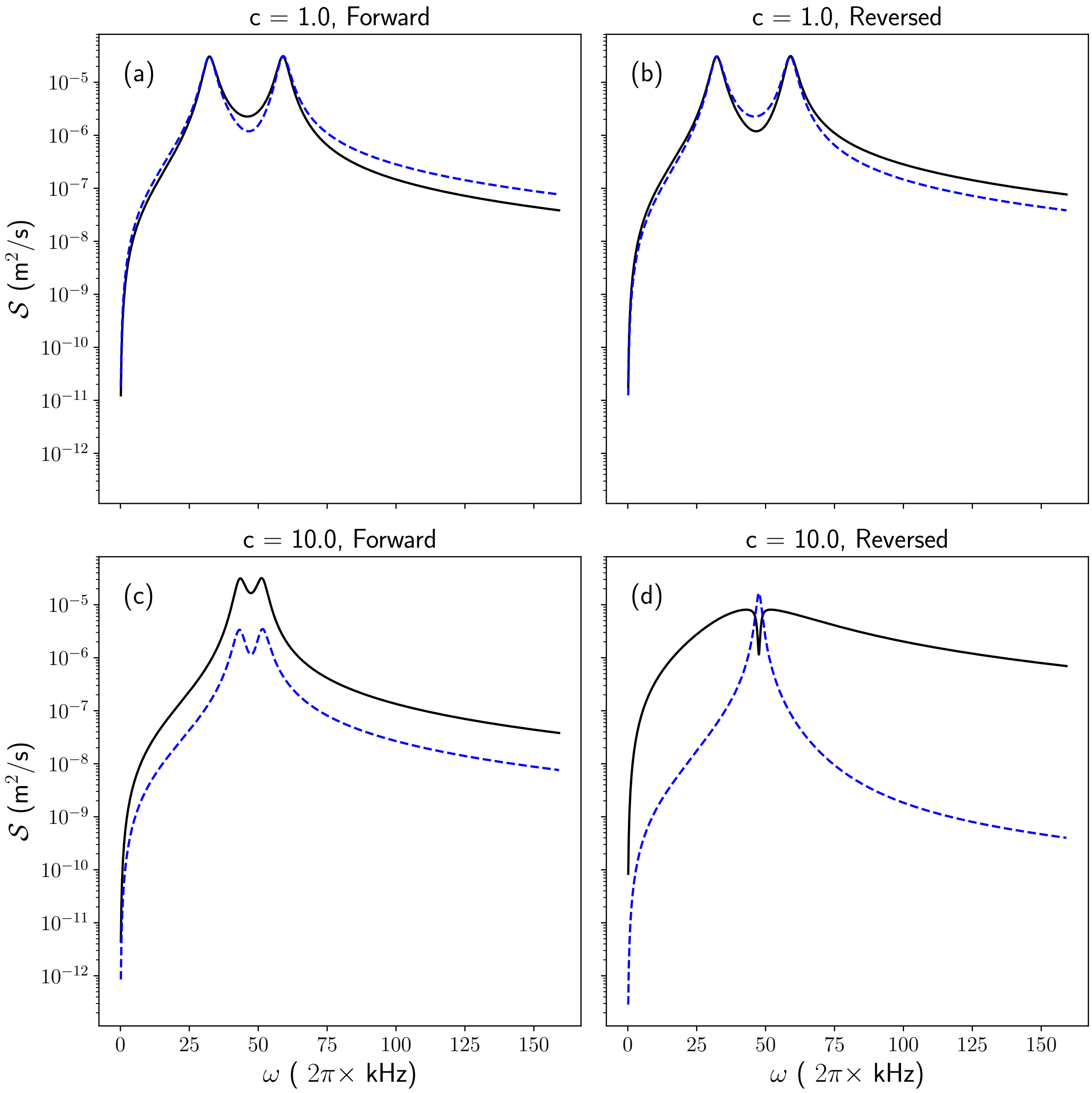

FIGURE 2.5: Spectral densities of the velocities of the ions (r_3 and r_4) corresponding to different values of c in Fig. 2.4: (a), (b) for $c = 1$ and (c), (d) for $c = 10$. Solid, black lines correspond to the left ion velocity spectral density $\mathbb{S}_{3,3}(\omega)$ and dashed, blue lines correspond to the right ion velocity spectral density $\mathbb{S}_{4,4}(\omega)$. (a) and (b) correspond to $R = 0$: the overlap between the phonon bands is the same in the forward and reversed configurations. (c) and (d) correspond to $R \approx 0.8$: in the forward configuration (c) the phonons match better than in the reversed configuration (d).

$m_1 C_{3,3}^{s.s.}/k_B$ and $T_2^{s.s.} = m_2 C_{4,4}^{s.s.}/k_B$).

For the vector process $\overrightarrow{r}(t)$ describing the evolution of our system we have $\overrightarrow{R}(\omega) = (i\omega - \mathbb{A})^{-1}\mathbb{L}\overrightarrow{\Xi}(\omega)$ with $\overrightarrow{\Xi}(\omega)$ being the Fourier transform of the white noise $\overrightarrow{\xi}(t)$. Note that $\overrightarrow{\Xi}(\omega)$ does not strictly exist, because it is not square-integrable, however its spectral density is $\mathbb{S}_{\overrightarrow{\xi}}(\omega) = 2\mathbb{D}$ [53], which is flat as expected for a white noise. Therefore, the spectral density matrix of the system is

$$\mathbb{S}_{\vec{r}} = 2\left(\mathbb{A} - i\omega\right)^{-1}\mathbb{L}\mathbb{D}\mathbb{L}^{\mathsf{T}}\left(\mathbb{A} + i\omega\right)^{-\mathsf{T}}. \tag{2.37}$$

As we can see in Eq. (2.37), the imaginary part of the eigenvalues of the dynamical matrix $\mathbb{A}$ correspond to the peaks in the spectrum whereas the real part dictates their width. The spectral density matrix of our model is

$$\mathbb{S}_{\vec{r}}(\omega) = 2k_B\frac{\gamma_L T_L \mathbb{S}_L(i\omega) + \gamma_L T_R \mathbb{S}_R(i\omega)}{(m_1 m_2)^2 P_{\mathbb{A}}(i\omega) P_{\mathbb{A}}(-i\omega)}, \tag{2.38}$$

where $P_{\mathbb{A}}(\lambda)$ is the characteristic polynomial of the dynamical matrix $\mathbb{A}$ and $\mathbb{S}_L(\omega)$, $\mathbb{S}_R(\omega)$ are the matrix polynomials in the angular frequency ω whose coefficients are defined in Appendix .2. Equation (2.39) gives the full expressions of the spectral densities for the velocities, $\mathbb{S}_{3,3}(\omega) = \langle R_3(\omega) R_3(-\omega)\rangle$ for the left ion, and $\mathbb{S}_{4,4}(\omega) = \langle R_4(\omega) R_4(-\omega)\rangle$ for the right ion, since they are the elements related to the calculation of the heat current using Eq. (2.36),

$$\begin{aligned}\mathbb{S}_{3,3}(\omega) &= 2k_B\frac{\gamma_R k^2 T_R \omega^2 + \gamma_L T_L\left[\omega^4\left(\gamma_R^2 - 2km_2 - 2k_R m_2\right) + \omega^2(k+k_R)^2 + m_2^2\omega^6\right]}{(m_1 m_2)^2 P_{\mathbb{A}}(i\omega) P_{\mathbb{A}}(-i\omega)},\\ \mathbb{S}_{4,4}(\omega) &= 2k_B\frac{\gamma_L k^2 T_L \omega^2 + \gamma_R T_R\left[\omega^4\left(\gamma_L^2 - 2km_1 - 2k_L m_1\right) + \omega^2(k+k_L)^2 + m_1^2\omega^6\right]}{(m_1 m_2)^2 P_{\mathbb{A}}(i\omega) P_{\mathbb{A}}(-i\omega)}.\end{aligned} \tag{2.39}$$

Figure 2.5 depicts a series of plots of the spectra given by Eq. (2.39) that correspond to two points in Fig. 2.4. For $c = 1$ (Fig. 2.5(a) and (b)) there is no rectification, since the spectra match in the forward (a) and reversed (b) configurations. However, for $c = 10$ ((Fig. 2.5(c) and (d))) the picture is very different: there is a good match between the spectra in the forward configuration whereas in the reversed configuration the spectra are less correlated, giving as a result higher rectification ($R \approx 0.8$). Figure 2.5 only shows the elements (3,3) and (4,4) in the diagonal of $\mathbb{S}$ but the remaining elements, including off-diagonal ones, exhibit a similar behavior.

2.7 Conclusions

We have studied heat rectification in a model composed of two coupled harmonic oscillators connected to baths. This simple model allows analytical treatment but still has enough complexity to examine different ingredients that can produce rectification. Our results demonstrate in a simple but realistic system that harmonic systems can rectificate heat current if they have features which depend on the temperature [21]. We implement this notion of temperature-dependent features by defining the baths exchange operation as an exchange of both temperatures and coupling parameters of the baths to the system. This kind of temperature-dependent features happens naturally in laser-cooled trapped ion set-ups.

We have also studied the phonon spectra of the system, comparing the match/mismatch of the phonon bands, to reach the conclusion that the band match/mismatch description for heat rectification is also valid for systems which are harmonic, as long as there are temperature-dependent features. We hope this article sheds more light into the topic of heat rectification and that encourages more research regarding its physical implementation on chains of trapped ions.

2.8 acknowledgements

We thank Daniel Alonso for fruitful discussions and comments. This work was supported by the Basque Country Government (Grant No. IT986-16), by Grants PGC2018-101355-B-I00 (MCIU/AEI/FEDER,UE) and FIS2016-80681P, and by the Spanish MICINN and European Union (FEDER) (Grant No. FIS2017-82855-P). M.A.S. acknowledges support by the Basque Government predoctoral program (Grant No. PRE-2019-2-0234).

.1 Full set of steady-state equations for the components of $\mathbb{C}^{s.s}$

Here we present the full set of equations for the covariance matrix elements in the steady state,

$$\begin{aligned}
\frac{2k\langle p_2q_1\rangle^{s.s.}}{m_1m_2}+\frac{2\gamma_L\langle p_1^2\rangle^{s.s.}}{m_1^3}&=\frac{2D_L}{m_1^2},\\
-\frac{2k\langle p_2q_1\rangle^{s.s.}}{m_2^2}+\frac{2\gamma_R\langle p_2^2\rangle^{s.s.}}{m_2^3}&=\frac{2D_R}{m_2^2},\\
-\frac{(k_L+k)\langle q_1q_2\rangle^{s.s.}}{m_1}+\frac{k\langle q_2^2\rangle^{s.s.}}{m_1}+\frac{\gamma_L\langle p_2q_1\rangle^{s.s.}}{m_1m_2}+\frac{\langle p_1p_2\rangle^{s.s.}}{m_1m_2}&=0,\\
\frac{(k_L+k)\langle p_2q_1\rangle^{s.s.}}{m_1m_2}-\frac{(k_R+k)\langle p_2q_1\rangle^{s.s.}}{m_2^2}+\frac{\gamma_L\langle p_1p_2\rangle^{s.s.}}{m_1^2m_2}+\frac{\gamma_R\langle p_1p_2\rangle^{s.s.}}{m_1m_2^2}&=0,\\
-\frac{(k_L+k)\langle q_1^2\rangle^{s.s.}}{m_1}+\frac{k\langle q_1q_2\rangle^{s.s.}}{m_1}+\frac{\langle p_1^2\rangle^{s.s.}}{m_1^2}&=0,\\
-\frac{(k_R+k)\langle q_2^2\rangle^{s.s.}}{m_2}+\frac{k\langle q_1q_2\rangle^{s.s.}}{m_2}+\frac{\langle p_2^2\rangle^{s.s.}}{m_2^2}&=0,\\
-\frac{(k_R+k)\langle q_1q_2\rangle^{s.s.}}{m_2}+\frac{k\langle q_1^2\rangle^{s.s.}}{m_2}-\frac{\gamma_R\langle p_2q_1\rangle^{s.s.}}{m_2^2}+\frac{\langle p_1p_2\rangle^{s.s.}}{m_1m_2}&=0
\end{aligned}\tag{40}$$

.2 Complete expressions for the Spectral Density Matrix

In Section 2.6 we used the characteristic polynomial $P_{\mathbb{A}}(\lambda)$ of the dynamical matrix $\mathbb{A}$ for the calculation of the spectral density matrix. $P_{\mathbb{A}}(\lambda)$ is defined as

$$\begin{aligned}
\det(\mathbb{A}-\lambda)=\lambda^4&\\
&+\lambda^3\left(\frac{\gamma_L}{m_1}+\frac{\gamma_R}{m_2}\right)\\
&+\lambda^2\frac{(\gamma_L\gamma_R+m_2(k+k_L)+m_1(k+k_R))}{m_1m_2}\\
&+\lambda\frac{(\gamma_R(k+k_L)+\gamma_L(k+k_R))}{m_1m_2}\\
&+\frac{k(k_L+k_R)+k_Lk_R}{m_1m_2}.
\end{aligned}\tag{41}$$

We also used the polynomials $\mathbb{S}_L(\lambda)$ and $\mathbb{S}_R(\lambda)$, which are defined as $\mathbb{S}_L(\lambda) = \sum_{n=0}^{6} \lambda^n \sim_{L,n}$ and $\mathbb{S}_R(\lambda) = \sum_{n=0}^{6} \lambda^n \sim_{R,n}$. There are 14 different polynomial coefficients, which are 4×4 matrices, which makes very cumbersome to include them in the main text. This is the full list of coefficients,

$$
\begin{aligned}
&\sim_{L,0} = \begin{pmatrix} (k+k_R)^2 & k(k+k_R) & 0 & 0 \\ k(k+k_R) & k^2 & 0 & 0 \\ 0 & 0 & 0 & 0 \\ 0 & 0 & 0 & 0 \end{pmatrix}, &&\sim_{R,0} = \begin{pmatrix} k^2 & k(k+k_L) & 0 \\ k(k+k_L) & (k+k_L)^2 & 0 \\ 0 & 0 & 0 \\ 0 & 0 & 0 \end{pmatrix} \\
&\sim_{L,1} = \begin{pmatrix} 0 & k\gamma_R & -(k+k_R)^2 & -k(k+k_R) \\ -k\gamma_R & 0 & -k(k+k_R) & -k^2 \\ (k+k_R)^2 & k(k+k_R) & 0 & 0 \\ k(k+k_R) & k^2 & 0 & 0 \end{pmatrix}, &&\sim_{R,1} = \begin{pmatrix} 0 & -k\gamma_L \\ k\gamma_L & 0 \\ k^2 & k(k+k_L) \\ k(k+k_L) & (k+k_L)^2 \end{pmatrix} \\
&\sim_{L,2} = \begin{pmatrix} 2(k+k_R)m_2-\gamma_R^2 & km_2 & 0 & -k\gamma_R \\ km_2 & 0 & k\gamma_R & 0 \\ 0 & k\gamma_R & -(k+k_R)^2 & -k(k+k_R) \\ -k\gamma_R & 0 & -k(k+k_R) & -k^2 \end{pmatrix}, &&\sim_{R,2} = \begin{pmatrix} 0 & km_1 \\ km_1 & 2(k+k_L)m_1-\gamma_L^2 \\ 0 & -k\gamma_L \\ k\gamma_L & 0 \end{pmatrix} \\
&\sim_{L,3} = \begin{pmatrix} 0 & 0 & \gamma_R^2-2(k+k_R)m_2 & -km_2 \\ 0 & 0 & -km_2 & 0 \\ 2(k+k_R)m_2-\gamma_R^2 & km_2 & 0 & -k\gamma_R \\ km_2 & 0 & k\gamma_R & 0 \end{pmatrix}, &&\sim_{R,3} = \begin{pmatrix} 0 & 0 \\ 0 & 0 \\ 0 & km_1 \\ km_1 & 2(k+k_L)m_1-\gamma_L^2 \end{pmatrix} \\
&\sim_{L,4} = \begin{pmatrix} m_2^2 & 0 & 0 & 0 \\ 0 & 0 & 0 & 0 \\ 0 & 0 & \gamma_R^2-2(k+k_R)m_2 & -km_2 \\ 0 & 0 & -km_2 & 0 \end{pmatrix}, &&\sim_{R,4} = \begin{pmatrix} 0 & 0 & 0 \\ 0 & m_1^2 & 0 \\ 0 & 0 & 0 \\ 0 & 0 & -km_1 \end{pmatrix} \\
&\sim_{L,5} = \begin{pmatrix} 0 & 0 & -m_2^2 & 0 \\ 0 & 0 & 0 & 0 \\ m_2^2 & 0 & 0 & 0 \\ 0 & 0 & 0 & 0 \end{pmatrix}, &&\sim_{R,5} = \begin{pmatrix} 0 & 0 & 0 & 0 \\ 0 & 0 & 0 & -m_1^2 \\ 0 & 0 & 0 & 0 \\ 0 & m_1^2 & 0 & 0 \end{pmatrix}, \\
&\sim_{L,6} = \begin{pmatrix} 0 & 0 & 0 & 0 \\ 0 & 0 & 0 & 0 \\ 0 & 0 & -m_2^2 & 0 \\ 0 & 0 & 0 & 0 \end{pmatrix}, &&\sim_{R,6} = \begin{pmatrix} 0 & 0 & 0 & 0 \\ 0 & 0 & 0 & 0 \\ 0 & 0 & 0 & 0 \\ 0 & 0 & 0 & -m_1^2 \end{pmatrix}.
\end{aligned}
\tag{42}
$$

Conclusions

My pleasure.

Appendix

Appendix A

Interaction versus asymmetry for adiabatic following

Extra information to add to your thesis.

Bibliography

[1] C. Starr, "*The Copper Oxide Rectifier*", Physics **7**, 15-19 (1936), `https://doi.org/10.1063/1.1745338`.

[2] M. Terraneo, M. Peyrard, and G. Casati, "*Controlling the Energy Flow in Nonlinear Lattices: A Model for a Thermal Rectifier*", Phys. Rev. Lett. **88**, 094302 (2002).

[3] E. Pereira, "*Thermal rectification in classical and quantum systems: Searching for efficient thermal diodes*", EPL (Europhysics Letters) **126**, 14001 (2019).

[4] N. Roberts and D. Walker, "*A review of thermal rectification observations and models in solid materials*", International Journal of Thermal Sciences **50**, 648 - 662 (2011).

[5] N. Li, J. Ren, L. Wang, G. Zhang, P. Hänggi, and B. Li, "*Colloquium: Phononics: Manipulating heat flow with electronic analogs and beyond*", Rev. Mod. Phys. **84**, 1045–1066 (2012).

[6] Z.-Q. Ye and B.-Y. Cao, "*Thermal rectification at the bimaterial nanocontact interface*", Nanoscale **9**, 11480-11487 (2017).

[7] L. Wang and B. Li, "*Thermal Memory: A Storage of Phononic Information*", Phys. Rev. Lett. **101**, 267203 (2008).

[8] L. Wang and B. Li, "*Thermal Logic Gates: Computation with Phonons*", Phys. Rev. Lett. **99**, 177208 (2007).

[9] B. Li, L. Wang, and G. Casati, "*Negative differential thermal resistance and thermal transistor*", Applied Physics Letters **88**, 143501 (2006).

[10] K. Joulain, J. Drevillon, Y. Ezzahri, and J. Ordonez-Miranda, "*Quantum Thermal Transistor*", Phys. Rev. Lett. **116**, 200601 (2016).

[11] C. W. Chang, D. Okawa, A. Majumdar, and A. Zettl, "*Solid-State Thermal Rectifier*", Science **314**, 1121–1124 (2006).

[12] W. Kobayashi, Y. Teraoka, and I. Terasaki, "*An oxide thermal rectifier*", Applied Physics Letters **95**, 171905 (2009).

[13] D. M. Leitner, "*Thermal Boundary Conductance and Thermal Rectification in Molecules*", The Journal of Physical Chemistry B **117**, 12820-12828 (2013).

[14] M. Elzouka and S. Ndao, "*High Temperature Near-Field NanoThermoMechanical Rectification*", Scientific Reports **7**, 44901 (2017).

[15] N. Li, P. Hänggi, and B. Li, "*Ratcheting heat flux against a thermal bias*", EPL (Europhysics Letters) **84**, 40009 (2008).

[16] B. Hu, L. Yang, and Y. Zhang, "*Asymmetric Heat Conduction in Nonlinear Lattices*", Phys. Rev. Lett. **97**, 124302 (2006).

[17] N. Zeng and J.-S. Wang, "*Mechanisms causing thermal rectification: The influence of phonon frequency, asymmetry, and nonlinear interactions*", Phys. Rev. B **78**, 024305 (2008).

[18] G. Katz and R. Kosloff, "*Quantum Thermodynamics in Strong Coupling: Heat Transport and Refrigeration*", Entropy **18**, (2016).

[19] G. Benenti, G. Casati, C. Mejía-Monasterio, and M. Peyrard, *From Thermal Rectifiers to Thermoelectric Devices*, pp. 365–407. Springer International Publishing, Cham, 2016.
`https://doi.org/10.1007/978-3-319-29261-8_10`.

[20] B. Li, L. Wang, and G. Casati, "*Thermal Diode: Rectification of Heat Flux*", Phys. Rev. Lett. **93**, 184301 (2004).

[21] E. Pereira, "*Requisite ingredients for thermal rectification*", Phys. Rev. E **96**, 012114 (2017).

[22] M. Pons, Y. Y. Cui, A. Ruschhaupt, M. A. Simón, and J. G. Muga, "*Local rectification of heat flux*", EPL (Europhysics Letters) **119**, 64001 (2017).

[23] M. Peyrard, "*The design of a thermal rectifier*", Europhysics Letters (EPL) **76**, 49–55 (2006).

[24] J. Wang, E. Pereira, and G. Casati, "*Thermal rectification in graded materials*", Phys. Rev. E **86**, 010101 (2012).

[25] S. Chen, E. Pereira, and G. Casati, "*Ingredients for an efficient thermal diode*", EPL (Europhysics Letters) **111**, 30004 (2015).

[26] M. Romero-Bastida, J. O. Miranda-Peña, and J. M. López, "*Thermal rectification in mass-graded next-nearest-neighbor Fermi-Pasta-Ulam lattices*", Phys. Rev. E **95**, 032146 (2017).

[27] N. Yang, N. Li, L. Wang, and B. Li, "*Thermal rectification and negative differential thermal resistance in lattices with mass gradient*", Phys. Rev. B **76**, 020301 (2007).

[28] M. Romero-Bastida and J. M. Arizmendi-Carvajal, "*Structural influences on thermal rectification of one-dimensional mass-graded lattices*", Journal of Physics A: Mathematical and Theoretical **46**, 115006 (2013).

[29] R. Dettori, C. Melis, R. Rurali, and L. Colombo, "*Thermal rectification in silicon by a graded distribution of defects*", Journal of Applied Physics **119**, 215102 (2016).

[30] E. Pereira, "*Graded anharmonic crystals as genuine thermal diodes: Analytical description of rectification and negative differential thermal resistance*", Phys. Rev. E **82**, 040101 (2010).

[31] E. Pereira, "*Sufficient conditions for thermal rectification in general graded materials*", Phys. Rev. E **83**, 031106 (2011).

[32] R. R. Ávila and E. Pereira, "*Thermal rectification features: a study starting from local assumptions*", Journal of Physics A: Mathematical and Theoretical **46**, 055002 (2013).

[33] D. Bagchi, "*Thermal transport in the Fermi-Pasta-Ulam model with long-range interactions*", Phys. Rev. E **95**, 032102 (2017).

[34] E. Pereira and R. R. Ávila, "*Increasing thermal rectification: Effects of long-range interactions*", Phys. Rev. E **88**, 032139 (2013).

[35] N. Freitas, E. A. Martinez, and J. P. Paz, "*Heat transport through ion crystals*", Physica Scripta **91**, 013007 (2015).

[36] A. Ruiz, D. Alonso, M. B. Plenio, and A. del Campo, "*Tuning heat transport in trapped-ion chains across a structural phase transition*", Phys. Rev. B **89**, 214305 (2014).

[37] A. Ruiz-García, J. J. Fernández, and D. Alonso, "*Delocalization and heat transport in multidimensional trapped ion systems*", Phys. Rev. E **99**, 062105 (2019).

[38] T. Pruttivarasin, M. Ramm, I. Talukdar, A. Kreuter, and H. Häffner, "*Trapped ions in optical lattices for probing oscillator chain models*", New Journal of Physics **13**, 075012 (2011).

[39] M. Ramm, T. Pruttivarasin, and H. Häffner, "*Energy transport in trapped ion chains*", New Journal of Physics **16**, 063062 (2014).

[40] J. I. Cirac and P. Zoller, "*A scalable quantum computer with ions in an array of microtraps*", Nature **404**, 579–581 (2000).

[41] F. N. Krauth, J. Alonso, and J. P. Home, "*Optimal electrode geometries for 2-dimensional ion arrays with bi-layer ion traps*", Journal of Physics B: Atomic, Molecular and Optical Physics **48**, 015001 (2014).

[42] R. Schmied, J. H. Wesenberg, and D. Leibfried, "*Optimal Surface-Electrode Trap Lattices for Quantum Simulation with Trapped Ions*", Phys. Rev. Lett. **102**, 233002 (2009).

[43] S. Lepri, R. Livi, and A. Politi, "*Thermal conduction in classical low-dimensional lattices*", Physics Reports **377**, 1 - 80 (2003).

[44] A. Dhar, "*Heat transport in low-dimensional systems*", Advances in Physics **57**, 457-537 (2008).

[45] R. Toral and P. Colet, *Stochastic numerical methods: an introduction for students and scientists*. John Wiley & Sons, 2014. `https://onlinelibrary.wiley.com/doi/abs/10.1002/9783527683147.ch6`.

[46] C. Cohen-Tannoudji, "*Atomic motion in laser light*", in *Fundamental systems in quantum optics*, J. Dalibard, J. M. Raimond, and J. Zinn-Justin, eds. Elsevier, 1992.

[47] H. J. Metcalf and P. van der Straten, "*Laser cooling and trapping of atoms*", J. Opt. Soc. Am. B **20**, 887–908 (2003).

[48] L. Chee Kong, "*Study of Classical and Quantum Open Systems*", arXiv:1008.0491.

[49] E. A. Novikov, "*Functionals and the random-force method in turbulence theory*", Soviet Journal of Experimental and Theoretical Physics **20**, 1290-1294 (1965).

[50] P.-W. Ma and S. L. Dudarev, "*Langevin spin dynamics*", Phys. Rev. B **83**, 134418 (2011).

[51] G. D. Chiara, G. Landi, A. Hewgill, B. Reid, A. Ferraro, A. J. Roncaglia, and M. Antezza, "*Reconciliation of quantum local master equations with thermodynamics*", New Journal of Physics **20**, 113024 (2018).

[52] A. Levy and R. Kosloff, "*The local approach to quantum transport may violate the second law of thermodynamics*", EPL (Europhysics Letters) **107**, 20004 (2014).

[53] S. Särkkä and A. Solin, *Applied Stochastic Differential Equations*. Institute of Mathematical Statistics Textbooks. Cambridge University Press, 2019.

[54] D. F. V. James, "*Quantum dynamics of cold trapped ions with application to quantum computation*", Applied Physics B **66**, 181–190 (1998).

[55] J. Bezanson, S. Karpinski, V. B. Shah, and A. Edelman, "*Julia: A Fast Dynamic Language for Technical Computing*", arXiv:1209.5145.

[56] J. Bezanson, A. Edelman, S. Karpinski, and V. Shah, "*Julia: A Fresh Approach to Numerical Computing*", SIAM Review **59**, 65-98 (2017).

[57] C. Rackauckas and Q. Nie, "*Adaptive methods for stochastic differential equations via natural embeddings and rejection sampling with memory*", Discrete and Continuous Dynamical Systems Series B **22**, 2731-2761 (2017).

[58] F. M. Leupold, *Bang-bang Control of a Trapped-Ion Oscillator*. PhD thesis, ETH Zurich, 2015. https://doi.org/10.3929/ethz-a-010616440.

[59] H.-Y. Lo, *Creation of Squeezed Schrödinger's Cat States in a Mixed-Species Ion Trap*. PhD thesis, ETH Zurich, 2015. https://doi.org/10.3929/ethz-a-010592649.

[60] T. Zhang and T. Luo, "*Giant Thermal Rectification from Polyethylene Nanofiber Thermal Diodes*", Small **11**, 4657-4665 (2015).

[61] M. Enderlein, T. Huber, C. Schneider, and T. Schaetz, "*Single Ions Trapped in a One-Dimensional Optical Lattice*", Phys. Rev. Lett. **109**, 233004 (2012).

[62] A. Bermudez, M. Bruderer, and M. B. Plenio, "*Controlling and Measuring Quantum Transport of Heat in Trapped-Ion Crystals*", Phys. Rev. Lett. **111**, 040601 (2013).

[63] C. Schneider, M. Enderlein, T. Huber, and T. Schaetz, "*Optical trapping of an ion*", Nature Photonics **4**, 772–775 (2010).

[64] A. Riera-Campeny, M. Mehboudi, M. Pons, and A. Sanpera, "*Dynamically induced heat rectification in quantum systems*", Phys. Rev. E **99**, 032126 (2019).

[65] H. Ma and Z. Tian, "*Significantly High Thermal Rectification in an Asymmetric Polymer Molecule Driven by Diffusive versus Ballistic Transport*", Nano Letters **18**, 43–48 (2018).

[66] K. M. Reid, H. D. Pandey, and D. M. Leitner, "*Elastic and Inelastic Contributions to Thermal Transport between Chemical Groups and Thermal Rectification in Molecules*", The Journal of Physical Chemistry C **123**, 6256-6264 (2019).

[67] T. J. Alexander, "*High-heat-flux rectification due to a localized thermal diode*", Phys. Rev. E **101**, 062122 (2020).

[68] Z. Rieder, J. L. Lebowitz, and E. Lieb, "*Properties of a Harmonic Crystal in a Stationary Nonequilibrium State*", Journal of Mathematical Physics **8**, 1073-1078 (1967).

[69] A. Casher and J. L. Lebowitz, "*Heat Flow in Regular and Disordered Harmonic Chains*", Journal of Mathematical Physics **12**, 1701-1711 (1971), https://doi.org/10.1063/1.1665794.

[70] M. A. Simón, S. Martínez-Garaot, M. Pons, and J. G. Muga, "*Asymmetric heat transport in ion crystals*", Phys. Rev. E **100**, 032109 (2019).

[71] D. Leibfried, R. Blatt, C. Monroe, and D. Wineland, "*Quantum dynamics of single trapped ions*", Rev. Mod. Phys. **75**, 281–324 (2003).

[72] S. Chu, L. Hollberg, J. E. Bjorkholm, A. Cable, and A. Ashkin, "*Three-dimensional viscous confinement and cooling of atoms by resonance radiation pressure*", Phys. Rev. Lett. **55**, 48–51 (1985).

[73] H. Metcalf and P. Van der Straten, *Laser Cooling and Trapping.* Graduate texts in contemporary physics. Springer-Verlag, New York, 1999.